

1

# Suitably impressive thesis title

2



3

Mikkel Bjørn

4

St. Anne's College

5

University of Oxford

6

A thesis submitted for the degree of

7

*Doctor of Philosophy*

8

Trinity 2020

## Acknowledgements

10 suitable thank you's

# Abstract

11

<sup>12</sup> World's best measurement of  $\gamma$ . Details to be added.

# Contents

13

14	<b>Preface</b>	vi
15	<b>1 Theoretical background</b>	1
16	1.1 The C, P and T symmetries and their violation . . . . .	1
17	1.2 CP violation in the Standard Model . . . . .	3
18	1.2.1 The CKM matrix and the Unitarity Triangle . . . . .	4
19	1.2.2 Measuring $\gamma$ in tree level decays . . . . .	7
20	1.3 Measuring $\gamma$ using multi-body D final states . . . . .	11
21	1.3.1 Dalitz plots and the phase space of multi-body decays . . . . .	11
22	1.3.2 The GGSZ method to measure $\gamma$ . . . . .	13
23	1.3.3 A model-independent approach . . . . .	15
24	1.3.4 Measuring strong-phase inputs at charm factories . . . . .	17
25	1.3.5 Global CP asymmetry and the relation to GLW and ADS measurements . . . . .	21
26	1.4 Strategy for the LHCb measurement . . . . .	25
28	<b>2 The LHCb experiment</b>	28
29	2.1 Subdetectors . . . . .	28
30	2.1.1 The VELO . . . . .	28
31	2.1.2 Magnet and tracking stations . . . . .	28
32	2.1.3 The RICH . . . . .	28
33	2.1.4 Calorimeters . . . . .	28
34	2.1.5 Muon detectors . . . . .	28
35	2.2 Track reconstruction . . . . .	28
36	2.3 The LHCb triggering system . . . . .	28
37	2.3.1 The level-0 hardware trigger . . . . .	28
38	2.3.2 High-level triggers . . . . .	28
39	2.3.3 Offline data filtering: the LHCb stripping . . . . .	28
40	2.4 Simulation . . . . .	28

41	<b>3 Neutral kaon <math>CP</math> violation and material</b>	<b>29</b>
42	<b>interaction in BPGGSZ measurements</b>	
43	3.1 CP violation and material interaction of neutral kaons . . . . .	29
44	3.1.1 A first look at the impact on $\gamma$ measurements . . . . .	33
45	3.2 Impact on BPGGSZ measurements of $\gamma$ :	
46	principles . . . . .	35
47	3.2.1 Modified symmetry relations . . . . .	35
48	3.2.2 Relationship between the $K_S^0$ and $K_L^0$ amplitudes . . . . .	36
49	3.2.3 Modification of the BPGGSZ yield equations . . . . .	37
50	3.3 Impact on BPGGSZ measurements of $\gamma$ :	
51	LHCb and Belle II measurements . . . . .	40
52	3.3.1 Detector geometries . . . . .	41
53	3.3.2 Kaon momentum distributions . . . . .	42
54	3.3.3 Experimental time acceptance . . . . .	43
55	3.3.4 Detector material budget . . . . .	44
56	3.3.5 Calculation procedure . . . . .	46
57	3.3.6 Results . . . . .	47
58	3.3.7 Coupled $B^\pm \rightarrow DK^\pm$ and $B^\pm \rightarrow D\pi^\pm$ measurements . . . . .	49
59	3.4 Concluding remarks . . . . .	50
60	<b>4 A GGSZ measurement with <math>B^\pm \rightarrow Dh^\pm</math> decays</b>	<b>52</b>
61	4.1 Candidate selection . . . . .	52
62	4.2 Signal and background components . . . . .	52
63	4.3 Measurement of the $CP$ -violation observables . . . . .	52
64	4.4 Systematic uncertainties . . . . .	52
65	4.5 Obtained constraints on $\gamma$ . . . . .	52
66	<b>Bibliography</b>	<b>53</b>

# Preface

67

68 The work presented in this thesis has been resulted in two papers, either under  
69 review or published in the Journal of High Energy Physics. These are

70 [1] *Measurement of the CKM angle  $\gamma$  using  $B^\pm \rightarrow [K_S^0 h^+ h^-]_D h^\pm$  decays*,  
71 submitted to JHEP.

72 This paper describes a measurement of the CKM angle  $\gamma$  using  $pp$  collision  
73 data taken with the LHCb experiment during the Run 1 of the LHC, in 2011  
74 and 2012, and during the full Run 2, in 2015–2018. The measurement uses the  
75 decay channels  $B^\pm \rightarrow D h^\pm$  where  $D \rightarrow K_S^0 h'^+ h'^-$ , in which  $h$  and  $h'$  denotes  
76 pions or kaons. It obtains a value of  $\gamma = (? \pm ?)^\circ$ , which constitutes the world’s  
77 best single-measurement determination of  $\gamma$ . The work is the main focus of  
78 this thesis and described in detail in Chapter 4.

79 [2] *CP violation and material interaction of neutral kaons in measurements*  
80 *of the CKM angle  $\gamma$  using  $B^\pm \rightarrow D K^\pm$  decays where  $D \rightarrow K_S^0 \pi^+ \pi^-$* , JHEP  
81 19 (2020) 106.

82 This paper describes a phenomenological study of the impact of neutral  
83 kaon  $CP$  violation and material interaction on measurements of  $\gamma$ . With the  
84 increased measurement precision to come in the near future, an understanding  
85 of these effects is crucial, especially in the context of  $B \rightarrow D\pi$  decays; however  
86 no detailed study had been published at the start of this thesis. The study is  
87 the subject of Chapter 3. Some text excerpts and figures from the paper have  
88 been reproduced in the thesis.

89 All of the work described in this thesis is my own, except where clearly referenced  
90 to others. Furthermore, I contributed significantly to an analysis of  $B^\pm \rightarrow D K^\pm$   
91 decays with LHCb data taken in 2015 and 2016, now published in

92 [3] *Measurement of the CKM angle  $\gamma$  using  $B^\pm \rightarrow D K^\pm$  with  $D \rightarrow K_S^0 \pi^+ \pi^-$*   
93  *$K_S^0 K^+ K^-$  decays*, JHEP 08 (2018) 176.

94 I was responsible for the analysis of the signal channel, whereas the control channel  
95 was analysed by Nathan Jurik. The measurement is superseded by that of Ref. [1]  
96 and is not described in detail in the thesis.

# 1

97

98

## Theoretical background

99 This chapter lays out the theoretical framework of the thesis. Section 1.1 introduces  
100 charge and parity symmetry violation in general, while Section 1.2 covers the  
101 description in the Standard Model and the general theory behind charge-parity  
102 symmetry violation measurements in charged  $B$  decays. Section 1.3 focuses on  
103 the theory of measurements using  $B^\pm \rightarrow Dh^\pm$  decays with multi-body  $D$  final  
104 states, after which the specific analysis strategy for the measurement described  
105 in the thesis is outlined out in Section 1.4.

106 **1.1 The C, P and T symmetries and their vio-  
107 lation**

108 The concept of symmetry play a fundamental role in modern physics. By Noether's  
109 theorem [4], the simple assumption of invariance of our physical laws under universal  
110 temporal and spatial translations leads to the very non-trivial prediction of conserved  
111 energy and momentum; within the field of particle physics, the interactions and  
112 dynamics of the Standard Model (SM) follow completely simply from requiring  
113 the fundamental particle fields to satisfy a local  $U(1) \times SU(2) \times SU(3)$  gauge  
114 symmetry [5]; and one of the short-comings of the SM, is that it fails to explain  
115 the apparent *lack* of symmetry in our matter-dominated universe [6]. Indeed, it is  
116 important to experimentally establish the symmetries of our world at a fundamental  
117 level, and the degree to which they are broken.

118 Three discrete symmetries of importance are the symmetries under

I'll  
adjust  
this para-  
graph  
when  
I've  
written  
the intro-  
duction.

- 119     1. The charge operator  $C$ , which conjugates all internal quantum numbers of a  
 120       quantum state and thus converts particles into their anti-particle counter parts.  
 121       For example,  $C$  transforms the electric charge of a particle state  $Q \rightarrow -Q$ .
- 122     2. The parity operator  $P$ , which inverts the spatial dimensions of space time:  
 123        $\vec{x} \rightarrow -\vec{x}$ . As such, it transforms left-handed particle fields into right-handed  
 124       particle fields and vice versa.
- 125     3. The time-inversion operator  $T$ , which inverts the temporal dimension of space  
 126       time:  $t \rightarrow -t$ .

127     These are fundamentally related by the *CPT* theorem [7] , which states that any  
 128       Lorentz-invariant Quantum Field Theory (QFT) must be symmetric under the  
 129       simultaneous application of *all* three operators. However, any one of the symmetries  
 130       can be broken individually, and experiments have shown the physical laws of our  
 131       world to violate each of the  $C$ ,  $P$ , and  $T$  symmetries.

132     Such a symmetry-breaking effect was established for the first time in 1956, when  
 133       Chien-Shiung Wu observed parity violation in weak decays of Co-60 nuclei [8], after  
 134       carrying out an experiment that was proposed by Yang Chen-Ning and Tsung-Dao  
 135       Lee [9]. While this experiment established the breaking of  $P$  symmetry, it left open  
 136       the possibility that the physical laws are invariant under a combination of a charge-  
 137       and parity inversion; that they are *CP* symmetric. However, this was disproved in  
 138       1964 when Kronin and Fitch observed that long-lived kaons, which predominantly  
 139       decay to the *CP*-odd  $3\pi$  state, could also decay to the *CP*-even  $\pi\pi$  states [10].

140     Since then *CP* violation has been found in the  $B^0$  system by the BaBar and Belle  
 141       collaborations [11, 12] during the early 2000's; the  $B$  factories, along with CDF, also  
 142       saw evidence for *CP* violation in  $B^\pm$  decays [13–18] later confirmed by LHCb [19],  
 143       and *CP* violation was measured for the  $B_s^0$  meson by LHCb in 2013 [20]; within the  
 144       last year and a half, the first observation of *CP*-violation in  $D^0$  decays has also been  
 145       made by the LHCb collaboration [21], and most recently evidence for *CP*-violation in  
 146       the neutrino sector has been reported by the T2K collaboration [22]. The observed  
 147       effects can be divided into distinct classes. The conceptually simplest case is

- 148     1. *CP-violation in decay*, where  $|A/\bar{A}| \neq 1$  for some decay amplitude  $A$ , and the  
 149       amplitude  $\bar{A}$  of the *CP*-conjugate decay. The result is different decay rates in  
 150       two *CP*-conjugate decays

$$\Gamma(M \rightarrow f) \neq \Gamma(\bar{M} \rightarrow \bar{f}). \quad (1.1)$$

This type of  $CP$  violation was not seen until the late 1980ies [23, 24], more than 20 years after the first observation of  $CP$  violation, and only finally established around the year 2000 [25, 26]. Also this discovery was made in  $K \rightarrow \pi\pi$  decays.

$CP$ -violation in decay is the only type possible for charged initial states, and it is thus the main focus of the thesis. Two additional  $CP$ -violating effect are possible for neutral initial states (a situation that will be the main focus of Chapter 3). These effects are

2.  $CP$ -violation in mixing, which denotes the case where the mixing rates between the  $M^0$  and  $\bar{M}^0$  states differ

$$\Gamma(M^0 \rightarrow \bar{M}^0) \neq \Gamma(\bar{M}^0 \rightarrow M^0). \quad (1.2)$$

The  $CP$  violation first observed by Kronin and Fitch in the neutral kaon sector [10] is (dominantly) of this type.

3.  $CP$ -violation in interference between mixing and decay, which can be present for a neutral initial states  $M^0$  decaying into a final state  $f$  common to both  $M^0$  and  $\bar{M}^0$ . The decay rate includes an interference term between two amplitudes: the amplitude for a direct  $M^0 \rightarrow f$  decay and the amplitude for a decay after mixing:  $M^0 \rightarrow \bar{M}^0 \rightarrow f$ . Even in the absence of the two aforementioned effects, the rates  $\Gamma(M^0 \rightarrow f)$  and  $\Gamma(\bar{M}^0 \rightarrow \bar{f})$  can differ due to the interference term. Such  $CP$  asymmetries have been measured in eg.  $B^0 \rightarrow J/\psi K$  by LHCb and the  $B$  factories, and in  $B_s^0 \rightarrow J/\psi \phi$  decays by the LHC and Tevatron experiments [27].

$CP$  violation measurements thus have a long, rich, and still-developing history.

## 1.2 CP violation in the Standard Model

All existing measurements of  $CP$  violation in the quark sector are naturally explained in the SM; indeed, the need to explain the observation  $CP$  violation in neutral kaons was a driving force in the development of the model in the first place, when it lead Kobayashi and Maskawa to predict the existence of then-unknown particles in 1973 [28] (now known to be the third generation quarks).

### 1.2.1 The CKM matrix and the Unitarity Triangle

The SM contains three generations of quarks, each consisting of an up-type quark ( $u$ ,  $c$ , and  $t$ ) and a down-type quark ( $d$ ,  $s$ , and  $b$ ). The charged weak interaction of the  $W^\pm$  boson couples up and down-type quarks. The quark states that couple to the  $W$  are not (a priori) identical to the mass eigenstates, and can be denoted  $(u', c', \text{ and } t')$  and  $(d', s', \text{ and } b')$ . A basis for the quark states can be chosen such that the weakly coupling up-quark states are identical to the propagating quark states,  $u = u'$ , but then the down-type quark state are different:  $d' \neq d$ . The two bases of the down-type quarks are related via the Cabibbo-Kobayashi-Maskawa (CKM) matrix [28, 29]<sup>1</sup>

$$\begin{pmatrix} d' \\ s' \\ t' \end{pmatrix} = V \begin{pmatrix} d \\ s \\ t \end{pmatrix} = \begin{pmatrix} V_{ud} & V_{us} & V_{ub} \\ V_{cd} & V_{cs} & V_{cb} \\ V_{td} & V_{ts} & V_{tb} \end{pmatrix} \begin{pmatrix} d \\ s \\ t \end{pmatrix}. \quad (1.3)$$

Thus the Lagrangian terms representing the coupling of a  $W^\pm$  boson with a  $u$ - and a  $d$ -type quark is

$$\mathcal{L}_{W^+} = -\frac{g}{\sqrt{2}} V_{ud} (\bar{u} \gamma^\mu W_\mu^+ d) \quad \mathcal{L}_{W^-} = -\frac{g}{\sqrt{2}} V_{ud}^* (\bar{d} \gamma^\mu W_\mu^- u) \quad (1.4)$$

where  $g$  is the weak coupling constant,  $\gamma_u$  are the Dirac matrices, and  $u$  and  $d$  represent the left-handed components of the physical quark states.

The CKM matrix is a unitary complex  $3 \times 3$  matrix, and hence has  $3^2 = 9$  independent, real parameters. However, 5 of these can be absorbed into non-physical phases of the quark states (both mass and weak eigenstates) and hence the matrix has 4 real, physical parameters: 3 mixing angles and a single phase. Chau and Keung [30] proposed the parameterisation

$$V = \begin{pmatrix} 1 & 0 & 0 \\ 0 & c_{23} & s_{23} \\ 0 & -s_{23} & c_{23} \end{pmatrix} \begin{pmatrix} c_{13} & 0 & s_{13}e^{-i\delta_{CP}} \\ 0 & 1 & 0 \\ -s_{13}e^{-i\delta_{CP}} & 0 & c_{13} \end{pmatrix} \begin{pmatrix} c_{12} & s_{12} & 0 \\ -s_{12} & c_{12} & 1 \\ 0 & 0 & 1 \end{pmatrix} \\ = \begin{pmatrix} c_{12}c_{13} & s_{12}c_{13} & s_{13}e^{-i\delta_{CP}} \\ -s_{12}c_{23} - c_{12}s_{23}s_{13}e^{i\delta_{CP}} & c_{12}c_{23} - s_{12}s_{23}s_{13}e^{i\delta_{CP}} & s_{23}c_{13} \\ s_{12}s_{23} - c_{12}c_{23}s_{13}e^{i\delta_{CP}} & -c_{12}s_{23} - s_{12}s_{23}s_{13}e^{i\delta_{CP}} & c_{23}c_{13} \end{pmatrix} \quad (1.5)$$

which is the preferred standard by the PDG [31]. Here,  $s_{ij} \equiv \sin \theta_{ij}$  and  $c_{ij} \equiv \cos \theta_{ij}$  denote the sine and cosine of three rotation angles in quark space;  $\theta_{12} = \theta_C$  being the usual Cabibbo angle [29].

<sup>1</sup> A basis for the quarks can of course be chosen, such that neither the up-quarks or the down-quarks are expressed in their mass eigenstates. In that case the CKM matrix is recovered as  $V = U_u^* U_d$ , where  $U_{u/d}$  is the unitary transformation matrices that brings the  $u/d$  quarks into their mass eigenstates.

The presence of the complex phase  $\delta_{CP}$  in the Lagrangian term of the  $W$  coupling causes  $CP$  violation because, as evident from Eq. (1.4), if  $\delta_{CP}$  enters the amplitude for some decay mediated by a  $W$  boson,  $A = |A|e^{i(\delta_0 + \delta_{CP})}$ , then it will enter the  $CP$  conjugate decay amplitude with the opposite sign:  $\bar{A} = |A|e^{i(\delta_0 - \delta_{CP})}$ . In these expressions,  $\delta_0$  denotes a  $CP$  conserving phase that is not caused by complex terms in the Lagrangian, but arises due to potential intermediate states in the decay amplitude.<sup>2</sup> Usually the underlying mechanism is due to QCD effects, and these  $CP$  conserving phases are therefore generally dubbed *strong* phases, as opposed to the  $CP$  violating *weak* phase of the  $W$  coupling [31]. This terminology will be applied throughout the thesis.

Experimentally, it has been observed that the CKM matrix elements of Eq. (1.5) satisfy  $s_{13} \ll s_{23} \ll s_{12}$ . This motivates an often used, alternative parameterisation of the matrix, where the elements are expressed as power series in a parameter  $\lambda$  that naturally incorporates this hierarchy: the Wolfenstein parameterisation [32].  
The definitions

$$\begin{aligned} s_{12} &\equiv \lambda \\ s_{23} &\equiv \lambda^2 A \\ s_{13} &\equiv \lambda^3 (\rho - i\eta) \end{aligned} \tag{1.6}$$

are made, after which the unitarity conditions (or Eq. 1.5) determine the remaining elements to any order in  $\lambda$ .<sup>3</sup> To  $\mathcal{O}(\lambda^5)$  the Wolfenstein parameterisation of the CKM matrix is [34, 35]

$$V = \begin{pmatrix} 1 - \frac{\lambda^2}{2} - \frac{\lambda^4}{8} & \lambda & A\lambda^3(\rho - i\eta) \\ -\lambda + \frac{\lambda^5}{2}A^2(1 - 2(\rho + i\eta)) & 1 - \frac{\lambda^2}{2} - \frac{\lambda^4}{8}(1 + 4A^2) & A\lambda^2 \\ A\lambda^3(1 - (\rho + i\eta)(1 - \frac{\lambda^2}{2})) & -A\lambda^2(1 - \frac{\lambda^2}{2}(1 - 2(\rho + i\eta))) & 1 - \frac{1}{2}A^2\lambda^4 \end{pmatrix}. \tag{1.7}$$

The unitarity condition  $V^\dagger V = \mathbb{1}$  of the CKM matrix defines 9 relations between the CKM elements of the form

$$\sum_j V_{jq}^* V_{jq} = 1 \quad , \quad q \in \{d, s, b\} \quad \text{along the diagonal} \tag{1.8a}$$

$$\sum_j V_{jq}^* V_{jq'} = 0 \quad , \quad q, q' \in \{d, s, b\}, q \neq q' \quad \text{off-diagonal.} \tag{1.8b}$$

---

<sup>2</sup>It is generally true that all phases of a single term in a given amplitude will be convention dependent, but that the phase differences between terms are not.

<sup>3</sup>Other variants of the Wolfenstein parameterisation do exist [33]. They all agree at the lowest orders of  $\lambda$ .

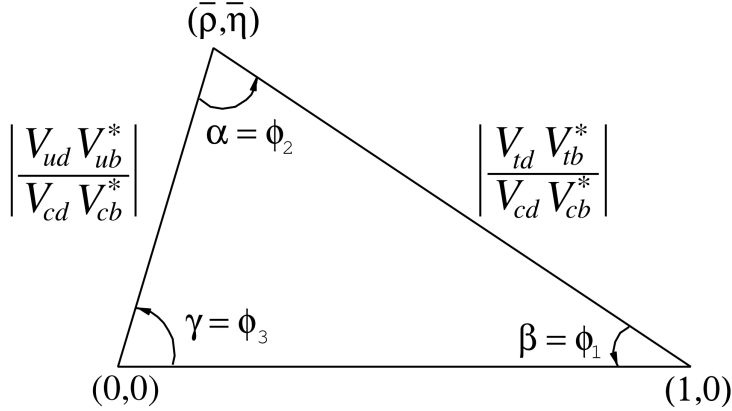


**Figure 1.1:** Definition of the lengths and sides of the Unitarity Triangle. Figure is taken from the *CKM Quark-Mixing Matrix* review of the PDG [31].

221 The off-diagonal conditions constrain three complex numbers to sum to zero, and  
 222 can thus be visualised as triangles in the complex plane, the so-called unitarity  
 223 triangles. Of these, the triangle corresponding to the  $(d, b)$  elements plays a  
 224 special role, because all three sides are of the same order of magnitude,  $\mathcal{O}(\lambda^3)$ .  
 225 When expressed in the form

$$\frac{V_{ud}^* V_{ub}}{V_{cd}^* V_{cb}} + \frac{V_{td}^* V_{tb}}{V_{cd}^* V_{cb}} + 1 = 0, \quad (1.9)$$

226 it is often referred to as the singular Unitarity Triangle, illustrated in Fig. 1.1 where  
 227 the usual names for the three angles are also given.

228 Over-constraining the unitarity triangle by making separate measurements of all  
 229 sides and angles, in as many different decay channels as possible, is an important,  
 230 and non-trivial test of the SM. The current experimental constraints are in agreement  
 231 with the SM predictions, as visualised in Fig. 1.2. The CKM angle

$$\gamma \equiv \arg(-V_{ud} V_{ub}^* / V_{cd} V_{cb}^*) = \arg(-V_{cb} V_{cd}^* / V_{ub} V_{ud}^*) \quad (1.10)$$

232 is unique among the CKM parameters, in that it can be measured in tree-level pro-  
 233 cesses without significant theoretical uncertainty from lattice QCD calculations [36].  
 234 Because tree-level processes are less likely to be affected by Beyond-Standard-Model  
 235 (BSM) effects, direct measurements of  $\gamma$  can be considered a SM benchmark, which  
 236 can be compared to estimates based on measurements of other CKM elements that  
 237 are measured in loop-level processes, and thus are more likely to be affected by  
 238 BSM effects [37]. The current, worldwide combination of direct measurements,  
 239 published by the CKMFitter group, is  $\gamma = (72.1^{+5.4}_{-5.7})^\circ$ , to be compared with the  
 240 estimate from loop-level observables of  $\gamma = (65.66^{+0.90}_{-2.65})^\circ$  [38]. Other world averages

Not sure if I should spend time explaining the non-gamma measurements entering?

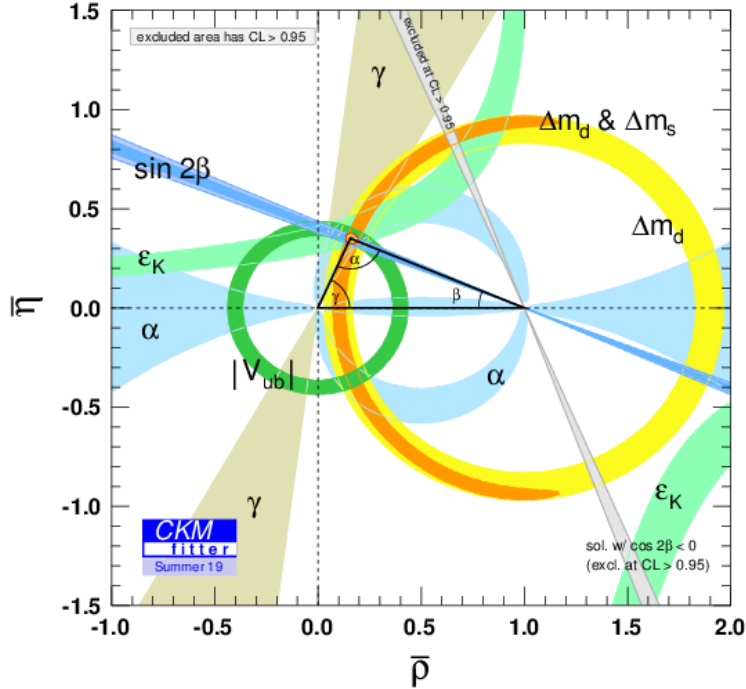


**Figure 1.2:** Current constraints on the Unitarity Triangle parameters as determined by the CKMFitter group for the EPS 2019 conference [38].

exist [27, 39], but the overall picture is the same: the ability to constrain BSM physics is currently limited by the uncertainty of the direct measurements. Hence further precision measurements of  $\gamma$  are highly motivated. Presently, the precision is driven by time-integrated measurements of direct  $CP$ -violation in  $B^\pm \rightarrow DK^\pm$  decays; such a measurement is the topic of this thesis and the theory behind is treated in detail in the following section. It is also possible to measure  $\gamma$  in time-dependent mixing analyses of  $B_s^0 \rightarrow D_s^\mp K^\pm$ ,  $B^0 \rightarrow D^\mp \pi^\pm$  and related decays, by measuring  $CP$  violation in interference between mixing and decay. These modes are expected to provide competitive measurements in the future [40, 41].

### 1.2.2 Measuring $\gamma$ in tree level decays

The phase  $\gamma$  can be measured in tree-level processes with interference between  $b \rightarrow c\bar{s}u$  and  $b \rightarrow \bar{c}s u$  transitions. The canonical example, also the subject of this thesis, is based on measurements sensitive to interference between the  $B^\pm \rightarrow D^0 K^\pm$  and  $B^\pm \rightarrow \bar{D}^0 K^\pm$  decay amplitudes. As illustrated in Fig. 1.3 for the case of  $B^-$  decays, the electro-weak phase difference between the two decays

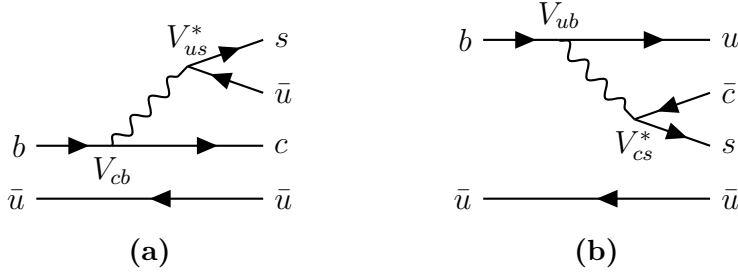


**Figure 1.3:** Tree level Feynman diagrams describing (a)  $B^- \rightarrow D^0 K^-$  and (b)  $B^- \rightarrow \bar{D}^0 K^-$  decays. The electro-weak phase difference between the two decays is  $\Delta\phi = \arg(V_{cb}V_{us}^*/V_{ub}V_{cs}^*) \simeq \gamma$ .

is  $\Delta\phi = \arg(V_{cb}V_{us}^*/V_{ub}V_{cs}^*)$ . While  $\Delta\phi$  is not identical to the definition of  $\gamma$  in Eq. (1.10), the ratio of the involved CKM matrix elements is [42]

$$\begin{aligned} -\frac{V_{cd}^*/V_{ud}^*}{V_{us}^*/V_{cs}^*} &= -\frac{-\lambda[1 - \frac{\lambda^4}{2}A^2(1 - 2(\rho - i\eta))](1 - \frac{\lambda^2}{2} - \frac{\lambda^4}{8}(1 + 4A^2))}{\lambda(1 - \frac{\lambda^2}{2} - \frac{\lambda^4}{4})} \\ &= 1 - \lambda^4 A^2(1 - 2(\rho - i\eta)) + \mathcal{O}(\lambda^5). \end{aligned} \quad (1.11)$$

The ratio equals unity to  $\mathcal{O}(\lambda^4) \simeq 2.6 \times 10^{-3}$ , and thus  $\Delta\phi \simeq \gamma$  is a good approximation within current experimental uncertainties. For the remainder of this thesis the approximation will be used without further comment. The diagrams in Fig. 1.3 describe the leading order contributions to the two amplitudes

$$\begin{aligned} A[B^- \rightarrow D^0 K^-] &\equiv A_B \\ A[B^- \rightarrow \bar{D}^0 K^-] &\equiv \bar{A}_B \equiv r_B A_B e^{i(\delta_B - \gamma)}, \end{aligned} \quad (1.12a)$$

where the last equality introduces two new parameters: the amplitude magnitude ratio  $r_B \equiv |\bar{A}_B|/|A_B|$ , and  $\delta_B$ , the strong-phase difference between the decay amplitudes. Since all  $CP$ -violation is attributed to the electro-weak phase in the SM, the  $CP$ -conjugate decay amplitudes are [43]

$$\begin{aligned} A[B^+ \rightarrow \bar{D}^0 K^+] &= A_B \\ A[B^+ \rightarrow D^0 K^+] &= \bar{A}_B = r_B A_B e^{i(\delta_B + \gamma)}. \end{aligned} \quad (1.12b)$$

In an experimental setting, the  $D^0$  and  $\bar{D}^0$  mesons are reconstructed in some final state,  $f$  or its  $CP$ -conjugate  $\bar{f}$ . In analogy with the  $B^\pm$  decays, the  $D$  decay amplitude can be related<sup>4</sup>

$$\begin{aligned} A[D^0 \rightarrow f] &= A[\bar{D}^0 \rightarrow \bar{f}] = A_D \\ A[\bar{D}^0 \rightarrow f] &= A[D^0 \rightarrow \bar{f}] = r_D A_D e^{i\delta_D}. \end{aligned} \quad (1.13)$$

<sup>4</sup>In this notation  $\delta_D$  is thus phase of the suppressed  $D$ -decay amplitude minus the phase of the favoured  $D$ -decay amplitude. This is the opposite convention to that used in the LHCb measurements with the ADS technique, but aligns with the notation used in the literature on  $\gamma$  measurements in  $D \rightarrow K_S^0 \pi^+ \pi^-$  decays.

where the assumption has been made that  $CP$  violation in the  $D$  decays is negligible, and  $\delta_D$  denotes a  $CP$ -conserving strong-phase difference. While  $CP$ -violation in  $D$  decays has recently been measured [21], the size of the effect is small and it is considered negligible in this thesis. Based on Eqs. 1.12 and (1.13), the decay rates of  $B^+$  and  $B^-$  mesons into the possible final states can be seen to satisfy

$$\Gamma(B^- \rightarrow D(\rightarrow f)K^-) \propto 1 + r_D^2 r_B^2 + 2r_B r_D \cos [\delta_B + \delta_D - \gamma], \quad (1.14a)$$

$$\Gamma(B^+ \rightarrow D(\rightarrow \bar{f})K^+) \propto 1 + r_D^2 r_B^2 + 2r_B r_D \cos [\delta_B + \delta_D + \gamma], \quad (1.14b)$$

$$\Gamma(B^- \rightarrow D(\rightarrow \bar{f})K^-) \propto r_D^2 + r_B^2 + 2r_B r_D \cos [\delta_B - \delta_D - \gamma], \quad (1.14c)$$

$$\Gamma(B^+ \rightarrow D(\rightarrow f)K^+) \propto r_D^2 + r_B^2 + 2r_B r_D \cos [\delta_B - \delta_D + \gamma]. \quad (1.14d)$$

The processes in Eqs. (1.14a) and (1.14b) are  $CP$ -conjugate and it is clear how, in the general case where  $\delta_B + \delta_D \neq 0$ , a non-zero value of  $\gamma$  leads to  $CP$  violation in the form of differing decay rates. The same is true for the processes in Eqs. (1.14c) and (1.14d). Depending on the choice of  $D$  final state, these expressions can be used to relate  $\gamma$  to various observables that are experimentally accessible. This thesis concerns the choice  $f = K_S^0 \pi^+ \pi^-$  or  $f = K_S^0 K^+ K^-$ , where the terms related to the  $D$  decay all have a non-trivial variation over the phase space of the decay. However, it is useful to first analyse the simpler case where  $f$  is a two-body state.

The simplest case is when  $f$  is chosen to be a  $CP$  eigenstate, so that  $f = \pm \bar{f}$  and the rate equations of (1.14a)–(1.14d) simplify, because  $r_D = 1$  and  $\delta_D \in \{0, \pi\}$ . Measurements of  $\gamma$  in such decay modes are denoted GLW measurements, after Gronau, London, and Wyler who described the approach in the early 90ies [43, 44]. Experimentally it is preferable to measure yield ratios rather than absolute rates, and the observables of interest are thus the  $CP$  asymmetry

$$\begin{aligned} A_{CP=\pm 1} &= \frac{\Gamma[B^- \rightarrow D_{CP} K^-] - \Gamma[B^+ \rightarrow D_{CP} K^+]}{\Gamma[B^- \rightarrow D_{CP} K^-] + \Gamma[B^+ \rightarrow D_{CP} K^+]} \\ &= \frac{\pm r_B \sin \delta_B \sin \gamma}{1 + r_B^2 \pm 2r_B \cos \delta_B \cos \gamma}, \end{aligned} \quad (1.15a)$$

as well as the ratio

$$\begin{aligned} R_{CP=\pm 1} &= 2 \frac{\Gamma[B^- \rightarrow D_{CP} K^-] + \Gamma[B^+ \rightarrow D_{CP} K^+]}{\Gamma[B^- \rightarrow D^0 K^-] + \Gamma[B^+ \rightarrow \bar{D}^0 K^+]} \\ &= 1 + r_B^2 \pm 2r_B \cos \delta_B \cos \gamma. \end{aligned} \quad (1.15b)$$

In practice,  $A_{CP}$  and  $R_{CP}$  are obtained from measured yield ratios that are corrected with appropriate branching fractions. A measurement of  $A_{CP}$  and  $R_{CP}$  alone is not sufficient to determine the underlying physics parameters  $(\gamma, r_B, \delta_B)$ , and this is not solely due to the number of parameters exceeding the number of constraints:

the equations also allow for multiple, ambiguous solutions for  $(\gamma, \delta_B)$ . One way to break the ambiguity, first noted in the original paper [43], is to make further measurements in additional  $B$  decays. These can be described with the formalism described above, but will not share the same ambiguous solutions because  $(r_B, \delta_B)$  are unique to a given  $B$  decay. Another method is to analyse  $D$  decay final states that are not  $CP$  eigenstates.

A few years later, Atwood, Dunietz, and Sonis analysed an alternative choice of  $D$  final states: a simultaneous analysis of a Cabibbo-favoured (CF) decay  $D^0 \rightarrow f$  and the doubly-Cabibbo-suppressed (DCS) decay  $D^0 \rightarrow \bar{f}$  into the  $CP$  conjugate final state [45, 46]. Their suggested method is named the ADS method after the authors. The classical example is to take  $f = K^-\pi^+$  and  $\bar{f} = \pi^-K^+$ . The relative suppression means that the  $r_D$  of Eq. (1.14) is small, typically of the same order of magnitude as  $r_B$ , and thus the  $CP$  asymmetry of the suppressed decay is  $\mathcal{O}(1)$ :

$$\begin{aligned} A_{ADS(\bar{f})} &= \frac{\Gamma[B^- \rightarrow D(\rightarrow \bar{f})K^-] - \Gamma[B^+ \rightarrow D(\rightarrow f)K^+]}{\Gamma[B^- \rightarrow D(\rightarrow \bar{f})K^-] + \Gamma[B^+ \rightarrow D(\rightarrow f)K^+]} \\ &= \frac{r_D r_B \sin(\delta_B - \delta_D) \sin \gamma}{r_D^2 + r_B^2 + 2r_D r_B \cos(\delta_B - \delta_D) \cos \gamma}. \end{aligned} \quad (1.16a)$$

The large  $CP$  asymmetry is a prime feature of the ADS method. However, also the suppressed-to-favoured yield ratio is sensitive to the physics parameters of interest:

$$\begin{aligned} R_{ADS(\bar{f})} &= \frac{\Gamma[B^- \rightarrow D(\rightarrow \bar{f})K^-] + \Gamma[B^+ \rightarrow D(\rightarrow f)K^+]}{\Gamma[B^- \rightarrow D(\rightarrow f)K^-] + \Gamma[B^+ \rightarrow D(\rightarrow \bar{f})K^+]} \\ &= \frac{r_B^2 + r_D^2 + 2r_D r_B \cos(\delta_B - \delta_D) \cos \gamma}{1 + r_D^2 r_B^2 + 2r_D r_B \cos(\delta_B + \delta_D) \cos \gamma}. \end{aligned} \quad (1.16b)$$

The interpretation of  $A_{ADS}$  and  $R_{ADS}$  in terms of  $(\gamma, r_B, \delta_B)$  requires knowledge of the  $r_D$  and  $\delta_D$  parameters, but these can be measured independently. In general, the constraints from a single set of ADS observables suffer the same ambiguities as in the GLW case. However, unlike the GLW case, each  $D$  decay mode provides an independent set of constraints, because the parameters related to the  $D$  decay vary.

The discussion of this section has centred on the classical case of  $B^\pm \rightarrow DK^\pm$  decays with a two-body  $D$  final state. With minor modifications the techniques have been used to make measurements of  $\gamma$  in  $B^0$  decays [?], with  $B$  decay final states including excited  $D$  mesons [?], excited kaons [?], or pions [?]. The decay  $B^\pm \rightarrow D\pi^\pm$  also is also  $CP$ -violating, although the effect is much smaller than in the  $B^\pm \rightarrow DK^\pm$  decay, because it is expected that  $r_B^{D\pi^\pm} \simeq 0.005$  [47], whereas  $r_B^{DK^\pm} \simeq 0.1$ . Furthermore, it is possible to use multi-body  $D$  final states. However, in some cases, a better precision can then be obtained by exploiting phase-space dependent decay rates. This is the topic of the next section.

### 322 1.3 Measuring $\gamma$ using multi-body D final states

323 In multi-body  $D$  decays, the  $r_D$  and  $\delta_D$  parameters of the fundamental rate equations  
 324 in Eq. (1.14) vary over the phase space of the  $D$  decay. This section describes a  
 325 model-independent approach to measure  $\gamma$  in  $B \rightarrow D(\rightarrow K_S^0\pi^+\pi^-)h^\pm$  decays by  
 326 exploiting this variation. The theory is identical for  $D \rightarrow K_S^0K^+K^-$  decays, and  
 327 similar ideas have been proposed for the  $D \rightarrow K_S^0\pi^+\pi^-\pi^0$  [48] and  $D \rightarrow 2\pi^+2\pi^-$   
 328 modes [49]. First, however, the formalism for describing amplitudes of multi-  
 329 body decays is briefly reviewed.

#### 330 1.3.1 Dalitz plots and the phase space of multi-body decays

331 In general, the phase space of the  $n$ -body decay  $P \rightarrow p_1 + p_2 + \dots + p_n$  consists of  $n$   
 332 four momenta, with a total of  $4n$  components. The requirement that each of the final  
 333 state particles is on-shell provides  $n$  constraints on these components, and energy-  
 334 momentum conservation removes a further 4 degrees of freedom. If the original  
 335 particle  $P$  is a scalar, the decay is isotropic, which removes an additional 3 degrees  
 336 of freedom, leaving the total number of degrees of freedom at  $3n - 7$ . For the specific  
 337 case of three-body decays, the available phase space can thus be parameterised with  
 338 only two parameters. A practical and often used choice is the invariant masses

$$s_{12} = m^2(p_1 p_2) = (p_1^\mu + p_2^\mu)^2, \quad s_{13} = m^2(p_1 p_3) = (p_1^\mu + p_3^\mu)^2. \quad (1.17)$$

339 The choice of particle pairs is arbitrary, and the coordinates easily related

$$m_P^2 + m_{p_1}^2 + m_{p_2}^2 + m_{p_3}^2 = m^2(p_1 p_2) + m^2(p_1 p_3) + m^2(p_2 p_3). \quad (1.18)$$

340 A scatter plot of  $(s_{12}, s_{13})$  values for a sample of particle decays is denoted a Dalitz  
 341 plot [50]. It has the very useful feature that the presence of (narrow) resonances  
 342 in the decay leads to visible bands in the scatter plot. Figure 1.4 illustrates how  
 343 the limits of the Dalitz plot are defined by kinematic constraints, and shows an  
 344 example of a Dalitz plot for  $D \rightarrow K_S^0\pi^+\pi^-$  decays in which the  $K^*(892)^\pm$  and  $\rho(770)$   
 345 resonances are clearly visible. The plot shows the sample of  $B^+ \rightarrow D\pi^+$  decays  
 346 used to make the measurement described in Chapter 4 and thus the  $D$  meson is in  
 347 a superposition of  $D^0$  and  $\bar{D}^0$  states (as detailed in the following section).

348 In terms of the coordinates of Eq. (1.17) the differential decay rate is given by

$$d\Gamma = \frac{1}{32(2\pi)^3 m_P^3} |\mathcal{M}|^2 ds_{12} ds_{13}, \quad (1.19)$$

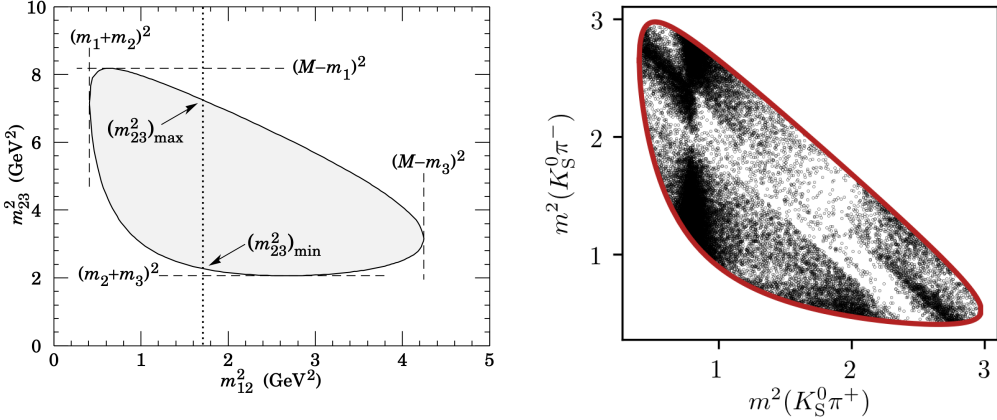


**Figure 1.4:** (Left) Schematic of a Dalitz plot and the limits of the kinematically allowed phase space limits. (Right) Example of a Dalitz plot for  $D \rightarrow K_S^0 \pi^+ \pi^-$  decays where the  $D$  meson originates in a  $B^+ \rightarrow D \pi^+$  decay; the decaying  $D$  meson is in a superposition of the  $D^0$  and  $\bar{D}^0$  states, but predominantly  $\bar{D}^0$ -like.

where  $\mathcal{M}$  is the QFT matrix element, or total decay amplitude, corresponding to the decay. In general, it is not possible to calculate  $\mathcal{M}$  from first principles. Instead, a model is defined with an empirically well motivated form, in which a number of free parameters must be determined experimentally. The simplest case is that of an *isobar* model, where it is assumed that the full decay can be decomposed into consecutive two-body decays of the form  $P \rightarrow R_{12}(\rightarrow p_1 + p_2)p_3$ . Thus,  $\mathcal{M}$  is expressed as a non-resonant constant amplitude term,  $k_{NR}$ , plus a sum of resonance terms

$$\mathcal{M}(s_{12}, s_{13}) = k_{NR} + \sum_r k_r \mathcal{M}^r(s_{12}, s_{13}). \quad (1.20)$$

The exact form of the  $\mathcal{M}^r$  function depends on the resonance in question. An overview is given in the PDG review on resonances and references therein [31]. The isobar formalism breaks down when resonances in the decay are not well separated. In this case, models of the form in Eq. (3.27) can still be employed, if the contribution from overlapping resonances are collected in a single term. An example of such a model, is the amplitude model for  $D^0 \rightarrow K_S^0 \pi^+ \pi^-$  decays developed by the Belle collaboration for a measurement of the CKM angle  $\beta$  in 2018 [51]. In this model, individual terms are included for  $D^0 \rightarrow K^*(\rightarrow K_S^0 \pi^\pm)\pi^\mp$  decays, whereas the  $\pi\pi$  and  $K\pi$   $S$ -wave contributions are modelled with the so-called  $K$ -matrix- and LASS formalisms [52, 53]. The amplitude and phase of  $\mathcal{M}$  as predicted by this model are shown in Fig. 1.5.

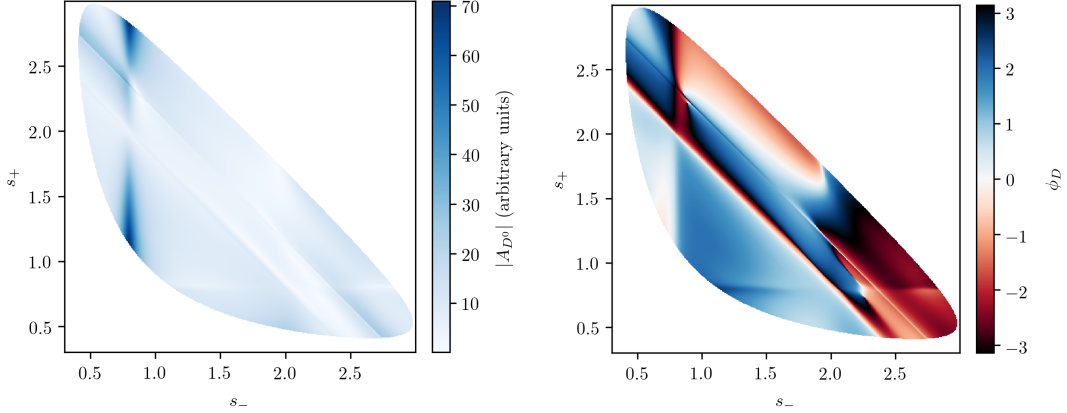


**Figure 1.5:** The (left) magnitude and (right) phase of the  $D \rightarrow K_S^0 \pi^+ \pi^-$  amplitude in the Belle 2018 model [51].

### 1.3.2 The GGSZ method to measure $\gamma$

The non-trivial phase-space dependence of the  $D \rightarrow K_S^0 \pi^+ \pi^-$  decay amplitude can be exploited to measure  $\gamma$  with  $B^\pm \rightarrow DK^\pm$  or  $B^\pm \rightarrow D\pi^\pm$  decays. This approach was proposed independently by Bondar [54], and by Giri, Grossman, Soffer, and Zupan [55] after whom it takes the commonly used acronym GGSZ. For this specific decay  $s_-$  and  $s_+$  are used to describe the Dalitz coordinates  $m^2(K_S^0 \pi^-)$  and  $m^2(K_S^0 \pi^+)$ , respectively, and the  $D$  decay amplitude is a function of these coordinates

$$A_S^{\bar{D}}(s_-, s_+) = A(\bar{D}^0 \rightarrow K_S^0 \pi^+ \pi^-). \quad (1.21)$$

To a good approximation the  $K_S^0$  meson is a  $CP$  eigenstate, meaning that the  $K_S^0 \pi^+ \pi^-$  state is self-conjugate. Assuming this approximation to be exact, and that  $CP$  violation in the  $D$  decay is negligible, the  $D$  decay amplitude satisfies the symmetry relation

$$A_S^{\bar{D}}(s_-, s_+) = A_S^D(s_+, s_-). \quad (1.22)$$

The impact of the  $K_S^0$  meson *not* being an exact  $CP$  eigenstate is treated in detail in Chapter 3. In order to simplify equations, the short-hand notation

$$(s_{-+}) = (s_-, s_+), \quad (s_{+-}) = (s_+, s_-), \quad (1.23)$$

will be employed for the remainder of the thesis, so that the relation in Eq. (1.22) can be expressed as  $A_S^{\bar{D}}(s_{-+}) = A_S^D(s_{+-})$ . Thus, the rate equations of Eq. (1.14)

382 for the  $D \rightarrow K_S^0\pi^+\pi^-$  decay mode are

$$\begin{aligned} d\Gamma^-(s_{-+}) &\propto |\mathcal{A}_S^-|^2 = |A_B|^2 |A_{K_S^0}|^2 \\ &\times [|A_S^D(s_{-+})|^2 + r_B^2 |A_S^D(s_{+-})|^2 + 2r_B |A_S^D(s_{-+})| |A_S^D(s_{+-})| \\ &\times (\cos[\delta_D(s_{-+})] \cos[\delta_B - \gamma] + \sin[\delta_D(s_{-+})] \sin[\delta_B - \gamma])], \end{aligned} \quad (1.24a)$$

$$\begin{aligned} d\Gamma^+(s_{-+}) &\propto |\mathcal{A}_S^+|^2 = |A_B|^2 |A_{K_S^0}|^2 \\ &\times [|A_S^D(s_{+-})|^2 + r_B^2 |A_S^D(s_{-+})|^2 + 2r_B |A_S^D(s_{-+})| |A_S^D(s_{+-})| \\ &\times (\cos[\delta_D(s_{-+})] \cos[\delta_B + \gamma] - \sin[\delta_D(s_{-+})] \sin[\delta_B + \gamma])]. \end{aligned} \quad (1.24b)$$

383 Here,  $\delta_D(s_{-+}) = \phi_D(s_{-+}) - \phi_D(s_{+-}) = -\delta_D(s_{+-})$ , where  $\phi_D(s_{-+})$  denotes the  
 384 complex phase of the  $A_S^D(s_{-+})$  amplitude, and a standard trigonometric relation  
 385 have been employed to factorise the terms depending on the complex phases of the  $B$   
 386 and  $D$  decays. It can be seen that in the case where  $\gamma = 0$  the  $B^+$  and  $B^-$  decay rates  
 387 are symmetric if the Dalitz coordinates are exchanged:  $\Gamma^+(s_-, s_+) = \Gamma^-(s_+, s_-)$ .  
 388 The presence of  $CP$  violation in the  $B$  decay breaks the symmetry. Therefore it is  
 389 possible to measure  $\gamma$  (and the nuisance parameters  $r_B$  and  $\delta_B$ ) from the phase-space  
 390 distribution of  $B^\pm \rightarrow D(\rightarrow K_S^0\pi^+\pi^-)K^\pm$  decays, given knowledge of  $A_S^D(s_{-+})$ .

391 A series of measurements of  $\gamma$  have been made that use amplitude models of the  
 392  $D$  decay [56–63]. However, a model-independent approach has been proposed by  
 393 Bondar and Poluektov [64, 65] that relies on binning phase-space, in which case the  
 394 necessary information on the  $D$  decay amplitude can be summarised in a small set  
 395 of coefficients that can be measured in a separate experiment. That is the approach  
 396 followed in this thesis, and has been used previously by the Belle [66] and LHCb  
 397 collaborations [67]. It is described in detail in the following section.

398 Such a model-independent approach is favourable for two reasons. Firstly,  
 399 uncertainty estimates related to model inputs and the choice of parameterisation in  
 400 an amplitude model are non-trivial, yet would become the leading systematic with  
 401 the very high precision expected for  $\gamma$  measurements in the near future. Secondly,  
 402 amplitude models are notoriously hard to reproduce, and in a high-precision era it  
 403 is favourable that any experiment is easy to reinterpret in various extensions of the  
 404 SM. This is a lot easier for an experiment that measures a small set of well-defined  
 405 observables, than for an experiment that fits a complicated amplitude model.

406 An alternative model-independent approach has recently been proposed by  
 407 Poluektov [68] where the externally measured input on the  $D$ -decay phase are  
 408 Fourier expansion coefficients, and which therefore avoids binning phase space; this  
 409 approach may have the potential to improve the obtainable precision in the future.

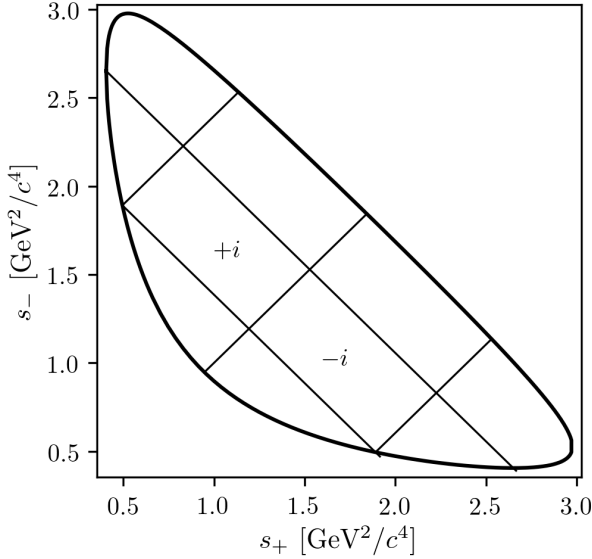


**Figure 1.6:** Illustration of the binning scheme used in GGSZ measurements: the bins are symmetric around the  $m^2(K_S^0\pi^+) = m^2(K_S^0\pi^-)$  diagonal, and numbered so that opposite bins have the same number, but with opposite sign.

### 410 1.3.3 A model-independent approach

411 The phase-space distribution can be analysed in a model-independent way, if the  
 412  $D$ -decay phase space is split into regions, or bins, an the  $B$  decay yield in each bin  
 413 determined experimentally. A measurement of  $\gamma$  using this approach is the main  
 414 topic of the thesis. This section describes the fundamental principle, whereas the  
 415 details pertaining to the exact experimental approach are delegated to Section 1.4.

416 The amplitude symmetry of Eq. (1.22) is exploited by defining  $2N$  bins to be  
 417 symmetric symmetric around the  $s_- = s_+$  diagonal of the Dalitz plot, numbered  
 418  $i = -N$  to  $N$  (omitting zero) such that if the point  $(s_-, s_+)$  is in bin  $i$ , then  $(s_+, s_-)$   
 419 is in bin  $-i$ , and by convention  $i > 0$  for bins where  $s_- > s_+$ . The principle  
 420 is illustrated in Fig. 1.6, but the binning schemes used in actual measurements  
 421 are more complicated. The decay rates in Eq. (1.24) can be integrated over such  
 422 bins, and give the bin yields

$$\begin{aligned} N_i^- &\propto h^- \left[ K_i + r_B^2 K_{-i} + 2\sqrt{K_i K_{-i}} (c_i x_- + s_i y_-) \right], \\ N_i^+ &\propto h^+ \left[ K_{-i} + r_B^2 K_i + 2\sqrt{K_i K_{-i}} (c_i x_+ - s_i y_+) \right], \end{aligned} \quad (1.25)$$

423 where the parameters describing the  $B$  decay have been expressed in terms of  
 424 the observables

$$x_\pm = r_B \cos(\delta_B \pm \gamma), \quad y_\pm = r_B \sin(\delta_B \pm \gamma), \quad (1.26)$$

and a number of phase-space integrated quantities related to the  $D$ -decay have been introduced. The  $K_i$  parameters denote fractional yield of a flavour-tagged  $D^0$  decaying into bin  $i$ , defined as

$$K_i = \frac{1}{N_K} \int_i ds^2 |A_S^D(s_{-+})|^2, \quad N_K = \int ds^2 |A_S^D(s_{-+})|^2, \quad (1.27)$$

where  $\int_i ds^2$  denotes integration over bin  $i$  of the Dalitz plot. The  $c_i$  and  $s_i$  denote the amplitude-weighted average of  $\cos \delta_D(s_{-+})$  and  $\sin \delta_D(s_{-+})$  over bin  $i$

$$\begin{aligned} c_i &= \frac{\int_i ds^2 |A_S^D(s_{-+})| |A_S^D(s_{+-})| \cos[\delta_D(s_{-+})]}{\sqrt{\int_i ds^2 |A_S^D(s_{-+})|^2} \sqrt{\int_i ds^2 |A_S^D(s_{+-})|^2}}, \\ s_i &= \frac{\int_i ds^2 |A_S^D(s_{-+})| |A_S^D(s_{+-})| \sin[\delta_D(s_{-+})]}{\sqrt{\int_i ds^2 |A_S^D(s_{-+})|^2} \sqrt{\int_i ds^2 |A_S^D(s_{+-})|^2}}. \end{aligned} \quad (1.28)$$

By the symmetry properties of  $\delta_D(s_{-+})$  these parameters satisfy  $c_i = c_{-i}$  and  $s_i = -s_{-i}$ . The normalisation constants  $h^+$  and  $h^-$  are identical in the ideal case, but it is convenient to define them separately for practical reasons: depending on the experimental setup, there may be overall production and detection asymmetries that affect the total signal yields. An experimental analysis can be made insensitive to these effects because they can be absorbed into the normalisation constants, as long as they are constant over the  $D$ -decay phase space. This comes at the cost that the information on  $x_\pm$  and  $y_\pm$  from the overall  $CP$  asymmetry is lost, but Section 1.3.5 will show the loss in precision to be minimal.

Thus, for a set of  $2N$  bins, the bin yields of Eqs. (1.25) provide  $4N$  constraints on a total of  $4N + 6$  parameters:  $(h^\pm, K_i, c_i, s_i, x_\pm, y_\pm)$ . However, the  $K_i$ ,  $c_i$ , and  $s_i$  parameters relate only to the  $D$  decay, and can thus, in principle, be measured in independent experiments. With such external inputs, a measurement of the  $B^\pm \rightarrow D(\rightarrow K_S^0 \pi^+ \pi^-) K^\pm$  yields in a set of bins can be used to constrain  $x_\pm$  and  $y_\pm$ , and thereby  $(\gamma, r_B, \delta_B)$ . The measurement presented in this thesis determines the  $K_i$  parameters directly, but uses externally measured values of  $c_i$  and  $s_i$  as input, as measured in quantum correlated  $D$  decays by the CLEO [69] and BESIII [70] collaborations. Because these measurements are the foundation of the approach, they are described in some detail in the following section. In the future, it is possible that the  $c_i$  and  $s_i$  parameters may be measured in quantum-correlated  $D$  decays in LHCb [71], and in charm-mixing measurements [72].

### 451 1.3.4 Measuring strong-phase inputs at charm factories

452 The strong-phase parameters  $c_i$  and  $s_i$  have been measured by the CLEO and  
 453 BESIII collaborations, using quantum correlated  $D^0\bar{D}^0$  pairs from decays of the  
 454  $\psi(3770)$  resonance state, itself produced in  $e^+e^-$  collisions at the resonance energy.  
 455 The  $\psi(3770)$  has quantum-number  $C = -1$ , which is conserved in the strong decay  
 456 into two  $D$  mesons, and thus the two  $D$  mesons are produced in an anti-symmetric  
 457 wave function. By observing the decay of one  $D$  meson into a specific final state,  
 458 say a  $CP$  eigenstate, the quantum state of the other  $D$  meson can be determined.  
 459 The measurement is based on decays where both  $D$  decays are reconstructed, one  
 460 in the  $K_S^0\pi^+\pi^-$  final state, the other in one of several different tag categories.  
 461 The main principles are outlined below, but most experimental considerations and  
 462 implementation details are left out for the sake of brevity.

463 The simplest case is when one  $D$  meson decays into a final state that uniquely  
 464 tags the flavour, such as  $\bar{D}^0 \rightarrow K^+e^-\bar{\nu}_e$ . In that case, the  $D$  meson decaying to  
 465  $K_S^0\pi^+\pi^-$  is known to be in the  $D^0$  state and the decay rate is simply determined by  
 466  $A_S^D : \Gamma(s_{-+}) \propto |A_S^D(s_{-+})|^2$ . This allows for a measurement of the  $K_i$  parameters.

467 If one  $D$  meson is reconstructed in a  $CP$ -even state, eg.  $K^+K^-$ , or a  $CP$ -odd  
 468 state, eg.  $K_S^0\pi^0$ , the  $D$  meson decaying to  $K_S^0\pi^+\pi^-$  is known to be in a state of  
 469 opposite  $CP$ . Thus, for a tag-decay of  $CP = \pm 1$  the decay rate has the form

$$\Gamma_{CP=\pm 1} \propto |A_S^D(s_{-+}) \mp A_S^D(s_{+-})|^2 \quad (1.29a)$$

470 and the bin yields will be given by

$$M_i^\pm \propto K_i + K_{-i} \mp 2\sqrt{K_i K_{-i}} c_i. \quad (1.29b)$$

471 Thus a simultaneous analysis of flavour and  $CP$  tagged decays allow for a deter-  
 472 mination of the  $K_i$  and  $c_i$  parameter sets.

473 Finally, the case where both  $D$  mesons, for now denoted  $D$  and  $D'$ , decay into  
 474 the  $K_S^0\pi\pi$  final state can be considered. The total amplitudes have contributions  
 475 from the case where  $D$  is in the  $D^0$  state and  $D'$  is in the  $\bar{D}^0$  state, as well as the  
 476 opposite flavour assignment. Thus the decay rate satisfies

$$\Gamma_{CP=\pm 1} \propto |A_S^D(s_{-+})A_S^D(s'_{+-}) + A_S^D(s_{+-})A_S^D(s'_{-+})|^2 \quad (1.30a)$$

477 where  $s_{-+}$  denotes the Dalitz-plot coordinates of the  $D$  meson, and  $s'_{-+}$  those of  
 478 the  $D'$  meson. Defining  $M_{ij}$  to be the yield of decays where the  $D$  decay is in  
 479 bin  $i$  and the  $D'$  in bin  $j$ , the bin yields satisfy

$$M_{ij} \propto K_i K_{-j} + K_j K_{-i} - 2\sqrt{K_i K_{-i} K_j K_{-j}} (c_i c_j + s_i s_j). \quad (1.30b)$$

480 Thus, analysing these decays in addition to the  $CP$  and flavour tagged decays provide  
 481 information on all of  $K_i$ ,  $c_i$ , and  $s_i$ . Note, however, that Eqs. (1.29) and (1.30) are  
 482 invariant under the transformation  $\delta_D \rightarrow -\delta_D$ . In practice, the analysis is extended  
 483 in a number of ways to enhance the statistics: using "flavour-tag" states that are not  
 484 exact flavour tags, such as  $K^-\pi^+$ , using self-conjugate multi-body  $D$ -decay final  
 485 states that are not exact  $CP$  eigenstates, such as  $\pi^+\pi^-\pi^0$ , and using the  $K_L^0\pi^+\pi^-$   
 486 final state as well. However, the main principles are the same as described above.

487 The measurements of  $c_i$  and  $s_i$  are made for a range of different binning schemes.  
 488 It was noted already in Ref. [65] that a rectangular binning scheme, such as the  
 489 example in Fig. 1.6, does not provide the optimal sensitivity to  $\gamma$ . A better sensitivity  
 490 can be obtained if the bins are defined such that  $\delta_D$  is approximately constant over  
 491 a given bin, by defining bin  $i$  out of  $N$  via the condition

$$\text{bin}_i = \{(s_-, s_+) \mid 2\pi(i - 3/2)/N < \delta_D(s_-, s_+) < 2\pi \times (i - 1/2)/N\}. \quad (1.31)$$

492 In practice, the binning scheme is defined by splitting the  $D$ -decay phase-space  
 493 into quadratic *micro bins* with a width of  $0.0054 \text{ (GeV}/c^2)^2$  and assigning a bin  
 494 number to each micro bin via the condition in (1.31) as evaluated in an amplitude  
 495 model of choice. The obtained binning scheme when using an amplitude model  
 496 developed by the BaBar collaboration in 2008 [57] is shown in Fig. 1.7a. In Ref [65]  
 497 it was also shown that the binning can be even further optimised for sensitivity.  
 498 The suggested figure of merit is

$$Q^2 = \frac{\sum_i \left( \frac{1}{\sqrt{N_i^B}} \frac{dN_i^B}{dx} \right)^2 + \left( \frac{1}{\sqrt{N_i^B}} \frac{dN_i^B}{dy} \right)^2}{\int ds^2 \left[ \left( \frac{1}{|\Gamma^B(s_-)|} \frac{d|\Gamma^B(s_-)|^2}{dx} \right)^2 + \left( \frac{1}{|\Gamma^B(s_-)|} \frac{d|\Gamma^B(s_-)|^2}{dy} \right)^2 \right]} \quad (1.32)$$

499 which quantifies the statistical sensitivity for a given binning, relative to the one  
 500 achievable in an unbinned analysis. The CLEO collaboration defined an *optimal*  
 501 binning scheme by an iterative procedure where, starting from the equal binning  
 502 scheme, a micro-bin is randomly reassigned new bin numbers in each step, and a  
 503 step accepted if  $Q^2$  increases. The optimisation is done for the case where  $x = y = 0$   
 504 and thus  $Q^2$  simplifies to  $Q_{x=y=0}^2 = \sum_i N_i^{x=y=0} (c_i^2 + s_i^2) / N_{total}^{x=y=0}$ . The resulting  
 505 binning scheme is shown in Fig. 1.7b. An additional binning scheme is defined,  
 506 denoted the *modified optimal* scheme and shown in Fig. 1.7c, where the  $Q^2$  figure  
 507 of merit is modified to take into account the presence of backgrounds [69]. The  
 508 modified optimal binning scheme has proven beneficial to use in measurements with  
 509 small signal yields [], but is not employed in the present thesis.

Where exactly is this phase sign known from?  
Is the overall sign not arbitrary in amplitude models?

**Table 1.1:** The experimentally measured  $c_i$  and  $s_i$  values used in the thesis. The  $D \rightarrow K_S^0\pi^+\pi^-$  values are the combined values from the BESIII and CLEO measurements published by BESIII [70]. The  $D \rightarrow K_S^0K^+K^-$  values are measured by CLEO [69].

Optimal binning scheme: $D \rightarrow K_S^0\pi^+\pi^-$		
Bin $i$	$c_i$	$s_i$
1	$-0.037 \pm 0.049$	$0.829 \pm 0.097$
2	$0.837 \pm 0.067$	$0.286 \pm 0.152$
3	$0.147 \pm 0.066$	$0.786 \pm 0.154$
4	$-0.905 \pm 0.021$	$0.079 \pm 0.059$
5	$-0.291 \pm 0.041$	$-1.022 \pm 0.062$
6	$0.272 \pm 0.082$	$-0.977 \pm 0.176$
7	$0.918 \pm 0.017$	$-0.184 \pm 0.065$
8	$0.773 \pm 0.033$	$0.277 \pm 0.118$

2-bins binning scheme: $D \rightarrow K_S^0K^+K^-$		
Bin $i$	$c_i$	$s_i$
1	$0.818 \pm 0.107$	$-0.445 \pm 0.215$
2	$-0.746 \pm 0.083$	$-0.229 \pm 0.220$

Both the CLEO and BESIII collaborations have measured the values of  $c_i$  and  $s_i$  for the equal, optimal, and modified optimal binning schemes. The results are also shown in Fig. 1.7, where they are compared to the expectation from the latest amplitude model [51]. The measurements presented in this thesis are based on a combination of the BESIII and CLEO results for the optimal binning scheme, made by the BESIII collaboration [70] and tabulated in Table 1.1.

While the *definition* and *optimisation* of these binning schemes depend on knowledge of  $A_S^D(s_-, s_+)$  via an amplitude model, it is important to note that no model information is needed when the binning schemes are used in the subsequent measurements of strong-phases<sup>5</sup> or  $CP$ -observables. Therefore the measurements will not be biased by any modelling imperfections, although the obtained precision might be lower than expected.

The preceding discussion has been focusing on the  $D \rightarrow K_S^0\pi^+\pi^-$  channel, however the  $D \rightarrow K_S^0K^+K^-$  channel can be analysed completely analogously. The CLEO collaboration measure  $c_i$  and  $s_i$  values for this mode as well, in three binning schemes [69]. These are all equal-phase binning schemes, with 2, 3, and 4 bins,

<sup>5</sup>With the exception of minimal model-dependence introduced when the  $K_L^0\pi^+\pi^-$  final state is employed to constrain the  $s_i$  parameters by the  $D$ -factories [69, 70], the impact of which is well under control.

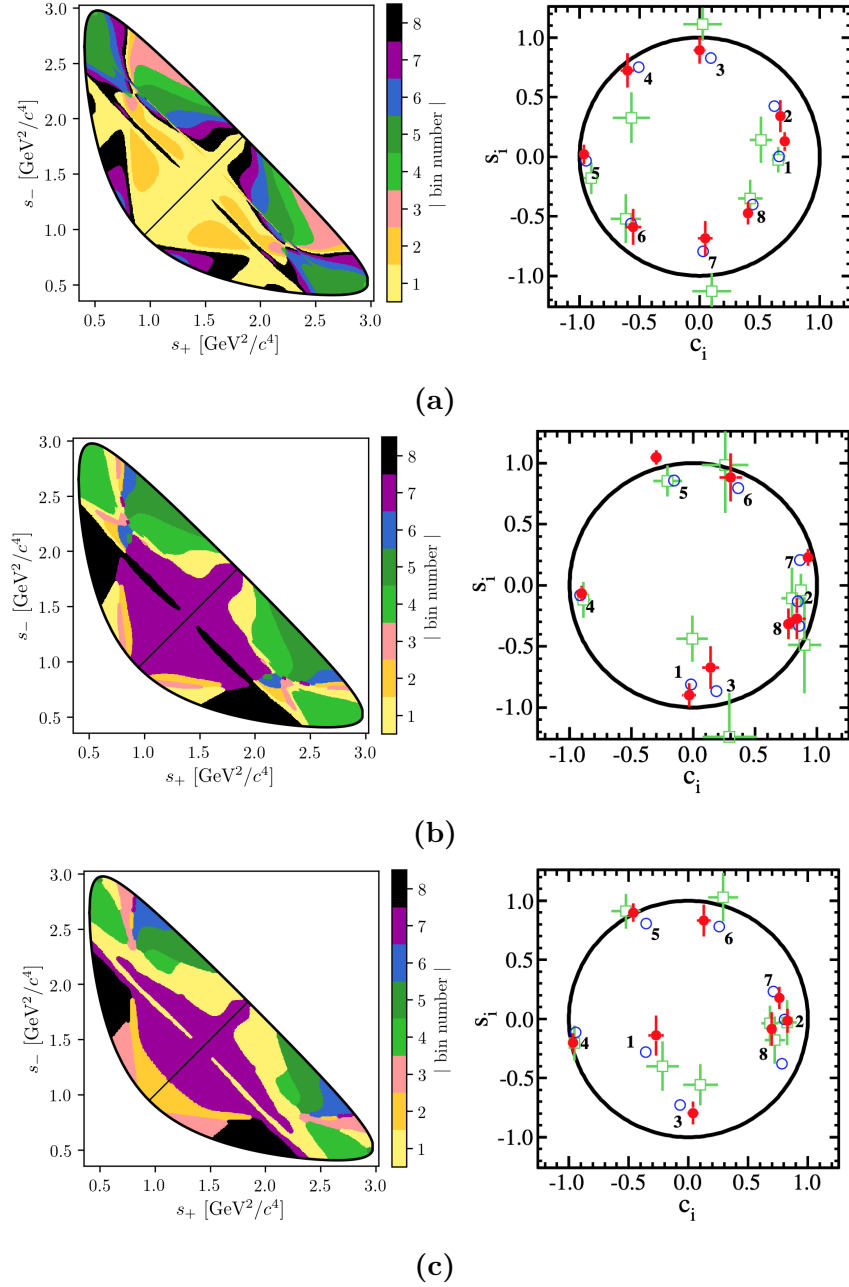


**Figure 1.7:** The (left) binning schemes and (right) measured values of  $(c_i, s_i)$  for (a) equal, (b) optimal, and (c) modified optimal binning schemes for  $D \rightarrow K_S^0 \pi^+ \pi^-$ . The plots of the measured values are taken from Ref. [70] and show the results obtained by (red) BESIII, (green) CLEO, and (blue) the model expectation using the model from Ref. [51]. The measurement featured in this thesis used the optimal binning scheme.

respectively, shown in Fig. 1.8. The  $D \rightarrow K_S^0 K^+ K^-$  decay amplitude is almost completely dominated by two  $K^+ K^-$  resonances, the  $CP$ -odd  $\phi(1020)$  and the  $CP$ -even  $a_0(980)$ , and this means that very little gain in sensitivity can be made by altering the equal-phase binning schemes. The measured  $c_i$  and  $s_i$  values are also shown in Fig. 1.8 and tabulated in Table 1.1 for the 2-bins scheme, which is used in this thesis. A BESIII measurement is in preparation, but has not been finished at the time of writing.

### 1.3.5 Global CP asymmetry and the relation to GLW and ADS measurements

The introduction of separate normalisation factors  $h^+$  and  $h^-$  in Eq. (1.25) hides the fact that information on  $\gamma$  (in principle) can be obtained from the asymmetry in phase-space-integrated  $B^+$  and  $B^-$  yields. In the ideal case where  $h^- = h^+$  the total yield asymmetry is

$$\begin{aligned} A_{GGSZ} &= \frac{\sum_i N_- - N_i^+}{\sum_{i=-N}^N N_i^- + N_i^+} = \frac{\sum_{i=-N}^N \sqrt{K_i K_{-i}} c_i (x_- - x_+)}{1 + r_B^2 + 2 \sum_{i=-N}^N \sqrt{K_i K_{-i}} c_i (x_- + x_+)} \\ &= \frac{2 \sum_{i=1}^N \sqrt{K_i K_{-i}} c_i (x_- - x_+)}{1 + r_B^2 + 4 \sum_{i=1}^N \sqrt{K_i K_{-i}} c_i (x_- + x_+)}, \end{aligned} \quad (1.33)$$

where it has been exploited that  $\sum_{i=-N}^N \sqrt{K_i K_{-i}} s_i = 0$  by definition. The size of the asymmetry is governed by the factor  $\sum_{i=1}^N \sqrt{K_i K_{-i}} c_i$ , which is small for  $D \rightarrow K_S^0 \pi^+ \pi^-$  and  $D \rightarrow K_S^0 K^+ K^-$  decays. The underlying reason is that  $\delta_D(s_-, s_+)$  varies significantly across phase-space for these decays, as evident by the spread in the values of  $c_i$  in Table 1.1, which reduces the *average* of the asymmetry-generating  $D^0 - \bar{D}^0$  interference term to being close to zero. The value of  $\sum_{i=-N}^N \sqrt{K_i K_{-i}} c_i$  is closely related to the  $CP$  content of the final state in question: for a self-conjugate  $CP$  even (odd) final state

$$A_{D^0}(s_-, s_+) = {}^{(+)}_{(-)} A_{\bar{D}^0}(s_-, s_+) = {}^{(+)}_{(-)} A_{D^0}(s_+, s_-) \quad (1.34)$$

and thus  $\sum_{i=1}^N \sqrt{K_i K_{-i}} c_i = {}^{(+)}_{(-)} 1$ . This motivates the definition of the  $CP$ -even fraction of the decay

$$\mathcal{F}_+ \equiv \frac{1}{2} \left( 1 + \sum_{i=1}^N \sqrt{K_i K_{-i}} c_i \right). \quad (1.35)$$

With  $\mathcal{F}_+$  in hand, the asymmetry in Eq. (1.33) can be rewritten

$$A_{GGSZ} = \frac{(2\mathcal{F}_+ - 1)r_B \sin \delta_B \sin \gamma}{1 + r_B^2(2\mathcal{F}_+ - 1)2r_B \cos \delta_B \cos \gamma}, \quad (1.36)$$

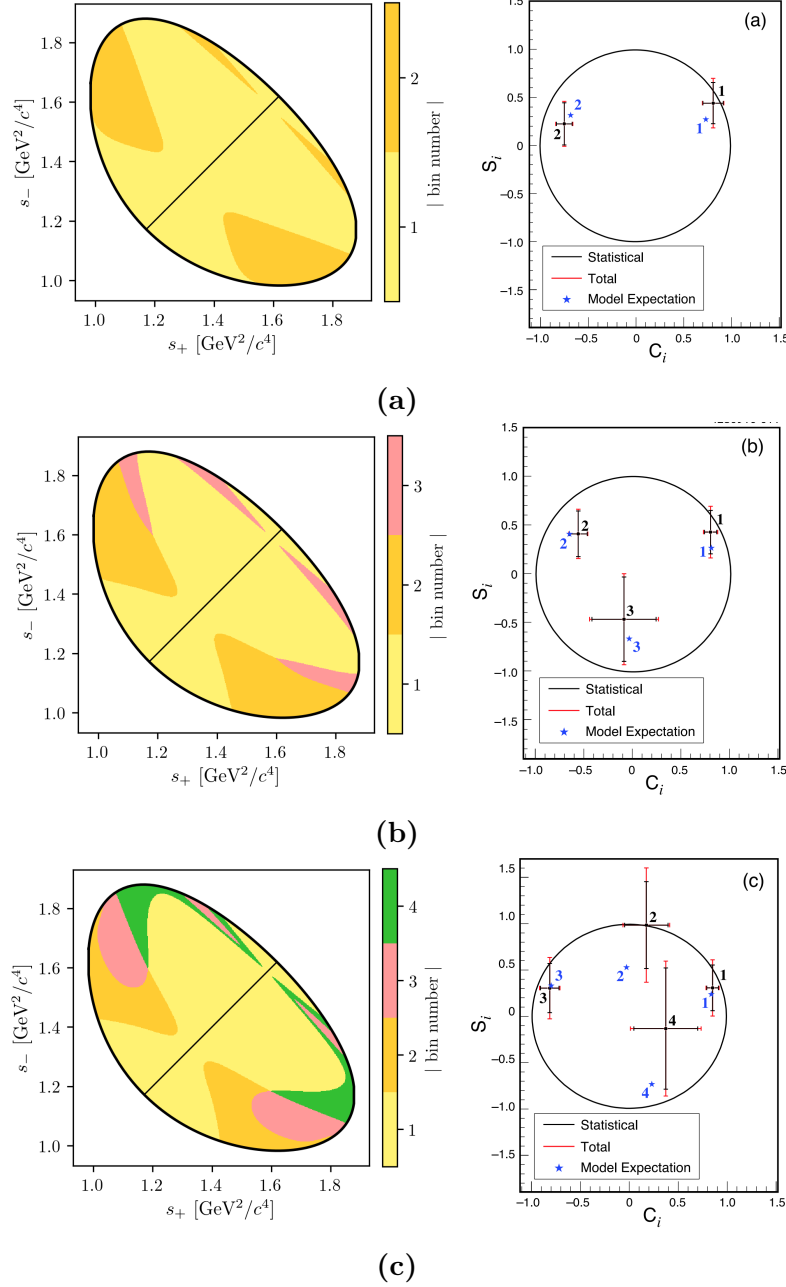


**Figure 1.8:** The (left) binning schemes and (right) measured values of  $(c_i, s_i)$  for the (a) 2-, (b) 3-, and (c) 4-bins binning schemes for  $D \rightarrow K_S^0 K^+ K^-$ . The plots of the measured values are taken from Ref. [69] and show the (error bars) results obtained by CLEO, and (blue) the model expectation using the model from Ref. [58]. The measurement featured in this thesis uses the 2-bins scheme.

which is the usual form used in quasi-GLW measurements []; for  $N = 1$  the definition in Eq. (1.35) is equivalent to  $\mathcal{F}_+$  as defined in Ref. []. The value of  $\mathcal{F}_+$  is independent of the number and shape of bins in a given binning scheme, as long as the bin definitions follow the symmetry principles outlined in Section 1.3.3. For  $D \rightarrow K_S^0\pi^+\pi^-$  and  $\bar{A}$  decays the values of  $\mathcal{F}_+$  are

$$\begin{aligned}\mathcal{F}_+(K_S^0\pi^+\pi^-) &= X? \\ \mathcal{F}_+(K_S^0K^+K^-) &= X?\end{aligned}\tag{1.37}$$

as evaluated with the Belle 2018 model for  $D \rightarrow K_S^0\pi^+\pi^-$  decays and the BaBar 2010 model for  $D \rightarrow K_S^0K^+K^-$  decays. Since  $r_B^{DK^\pm} \sim 0.1$  the predicted global asymmetries are thus approximately 1–2 %, which is not resolvable with the current experimental yields. As shown in Chapter 3,  $CP$  violation in the  $K_S^0$  sector leads to asymmetries of a similar size, further complicating the use of global asymmetries to constrain  $x_\pm$  and  $y_\pm$ . Thus these modes are ill-suited for quasi-GLW measurements, and ignoring global asymmetries leads to a negligible loss of information on  $\gamma$  in a GGSZ measurement. The reverse is true for a well-suited quasi-GLW mode, such as  $D \rightarrow \pi^+\pi^-\pi^0$ : if  $\mathcal{F}_+$  is close to either zero or unity, it means that  $(c_i, s_i)$  will be close to  $(\pm 1, 0)$  in all bins for *any* given binning scheme, and the set of bins will provide almost identical constraints on  $x_\pm$  and  $y_\pm$ . Thus, the binning of phase space leads to no significant gain in precision compared to a global analysis.

Indeed, a crucial quality of the GGSZ method, is that exactly because each bin-pair provides independent constraints on  $x_\pm$  and  $y_\pm$ , the method provides a single solution for  $(\gamma, r_B, \delta_B)$  that does not suffer the ambiguities of the ADS and GLW approaches. In order to illustrate this further, it is useful to make one more comparison of the model-independent GGSZ formalism to the ADS and GLW formalisms. If there was no  $CP$  symmetry the  $B^+$  yield in bin  $+i$  would equal the  $B^-$  yield in bin  $-i$ . Therefore the relevant  $CP$  asymmetry for a given Dalitz bin is

$$\begin{aligned}A_{GGSZ}^i &\equiv \frac{N_i^- - N_{-i}^+}{N_i^- + N_{-i}^+} \\ &= \frac{\sqrt{K_i K_{-i}}(c_i(x_- - x_+) + s_i(y_- - y_+))}{K_i + r_B^2 K_{-i} + 2\sqrt{K_i K_{-i}}(c_i(x_- + x_+) + s_i(y_- + y_+)})\end{aligned}\tag{1.38}$$

This expression is identical to the ADS asymmetry in Eq. (1.16a) if the effective  $D$ -decay parameters  $r_D^i$  and  $\delta_D^i$  are defined via

$$\kappa_i \cos \delta_D^i \equiv c_i \quad , \quad \kappa_i \sin \delta_D^i \equiv s_i \quad , \quad r_D^i \equiv \sqrt{K_i/K_{-i}},\tag{1.39}$$

and a coherence factor,  $\kappa$ , is included in the interference terms of the ADS expression, as is standard for multi-body  $D$  decays []. These parameters allow us to classify

**Table 1.2:** Classification of the bins used in model-independent GGSZ measurements, in terms of whether the interplay between the  $D^0$  and  $\bar{D}^0$  amplitudes in the bin resemble typical GLW or ADS behaviour. The parameters are calculated using the 2018 Belle model [1] for  $D \rightarrow K_S^0\pi^+\pi^-$  decays and the 2010 BaBar model [2] for  $D \rightarrow K_S^0K^+K^-$  decays.

Optimal binning scheme: $D \rightarrow K_S^0\pi^+\pi^-$					
Bin $i$	$\hat{r}_D$	$\hat{\delta}_D$	$\mathcal{F}_+$	$\kappa$	Bin type
1	0.473	91.9°	48.97 %	0.81	Mixed
2	0.164	11.1°	63.38 %	0.85	ADS-like
3	0.157	79.4°	52.50 %	0.89	ADS-like
4	0.768	175.3°	5.85 %	0.92	GLW-odd-like
5	0.759	-99.9°	42.84 %	0.87	Mixed
6	0.223	-64.5°	57.92 %	0.87	ADS-like
7	0.651	-13.3°	89.44 %	0.89	GLW-even-like
8	1.745	21.0°	87.08 %	0.92	GLW-even-like

2-bins binning scheme: $D \rightarrow K_S^0K^+K^-$					
Bin $i$	$\hat{r}_D$	$\hat{\delta}_D$	$\mathcal{F}_+$	$\kappa$	Bin type
1	0.816	19.8°	86.14 %	0.78	GLW-even-like
2	0.775	154.5°	16.23 %	0.77	GLW-odd-like

578 a given pair of bins with number  $\pm i$  as either *GLW-like*, if  $\delta_D^i$  is close to 0 or  $\pi$   
 579 and  $r_D^i$  is close to unity, or *ADS-like* if  $0 < r_D^i \ll 1$ . The  $CP$ -even fraction of the  
 580  $D$ -decay can also be defined for a given bin-pair:

$$\mathcal{F}_+^i = \mathcal{F}_+^{-i} \equiv \frac{1}{2} \left( 1 + 2c_i \frac{\sqrt{K_i K_{-i}}}{K_i + K_{-i}} \right) = \frac{1}{2} \left( 1 + 2c_i \frac{r_D^i}{1 + r_D^{i/2}} \right). \quad (1.40)$$

581 A GLW-even-like bin pair will have  $\mathcal{F}_+^i \simeq 1$  and a GLW-odd-like bin pair will  
 582 have  $\mathcal{F}_+^i \simeq 0$ .

583 Table 1.2 summarises a classification of the bins for the optimal  $D \rightarrow K_S^0\pi^+\pi^-$   
 584 binning scheme and the 2-bins  $D \rightarrow K_S^0K^+K^-$  binning scheme following these  
 585 principles. Two bins are classified as *mixed* because  $r_D^i$  is not particularly small,  
 586 but  $\mathcal{F}_+^i$  is close to 0.5. The fact that multiple bin types appear for both the  
 587  $D \rightarrow K_S^0\pi^+\pi^-$  and  $D \rightarrow K_S^0K^+K^-$  modes underline that each mode benefits from  
 588 being analysed in the GGSZ formalism, and that the bins provide independent  
 589 constraints, allowing for a non-ambiguous solution for  $(\gamma, r_B, \delta_B)$ .

## 590 1.4 Strategy for the LHCb measurement

591 The main topic of the thesis is a model-independent GGSZ measurement using  
 592  $B^\pm \rightarrow DK^\pm$  and  $B^\pm \rightarrow D\pi^\pm$  decays, and the two  $D$  final states  $K_S^0\pi^+\pi^-$  and  
 593  $K_S^0K^+K^-$ . The measurement uses the optimal binning scheme for the  $D \rightarrow K_S^0\pi^+\pi^-$   
 594 mode, with the combined strong-phase inputs from the BESIII [70] and CLEO [69]  
 595 collaborations published in Ref. [70]. For the  $D \rightarrow K_S^0K^+K^-$  channel, the 2-  
 596 bins scheme is used with the strong-phase parameters measured by the CLEO  
 597 collaboration [69]. The details of the analysis are presented in Chapter (4), but  
 598 the overall strategy and a few extensions of the formalism from the previous  
 599 sections are given here.

600 Due to the geometry of the LHCb detector, the signal reconstruction efficiency  
 601 for  $B^\pm \rightarrow D(\rightarrow K_S^0h^+h^-)h'^\pm$  decays varies significantly across the  $D$ -decay phase  
 602 space. Denoting the efficiency profile as  $\eta(s_-, s_+)$ , the yield equations of Eq. (1.25)  
 603 are therefore modified slightly

$$604 N_i^- = h^{B^-} \left[ F_i + r_B^2 F_{-i} + 2\sqrt{F_i F_{-i}} (c'_i x_- + s'_i y_-) \right], \\ N_i^+ = h^{B^+} \left[ F_{-i} + r_B^2 F_i + 2\sqrt{F_i F_{-i}} (c'_i x_+ - s'_i y_+) \right], \quad (1.41)$$

604 where the phase-space integrated quantities now include the efficiency profile

$$605 F_i = \frac{1}{N_F} \int ds^2 \eta(s_{-+}) |A_S^D(s_{-+})|^2, \quad N_F = \int ds^2 \eta(s_{-+}) |A_S^D(s_{-+})|^2, \quad (1.42)$$

$$605 c'_i = \frac{\int_i ds^2 \eta(s_{-+}) |A_S^D(s_{-+})| |A_S^D(s_{-+})| \cos[\delta_D(s_{-+})]}{\sqrt{\int_i ds^2 \eta(s_{-+}) |A_S^D(s_{-+})|^2} \sqrt{\int_i ds^2 \eta(s_{-+}) |A_S^D(s_{-+})|^2}}, \quad (1.43)$$

606 with an analogous definition of  $s'_i$ . At leading order, the strong-phase parameters are  
 607 unaffected by the non-uniform efficiency, and, in addition, the bin definitions favour  
 608 bins for which  $c_i$  and  $s_i$  take on similar values across each bin. Therefore, the  $c_i$   
 609 and  $s_i$  values reported by the charm factories are used directly in the measurement.  
 610 The impact on the obtained central values is negligible, as described in detail in  
 611 Section 4.4 where a systematic uncertainty is assigned.

612 The  $F_i$  are significantly different to the  $K_i$  due to the experimental acceptance  
 613 profile in LHCb. Given external inputs for the strong-phase parameters, it is  
 614 possible to fit the  $F_i$  parameters and  $x_\pm$  and  $y_\pm$  simultaneously in a fit to the  
 615 LHCb  $B^\pm \rightarrow DK^\pm$  data set, in which case the obtained  $F_i$  parameters incorporate  
 616 the correct acceptance profile correction by construction. However, the obtainable  
 617 precision for the  $CP$  observables measured by this procedure is suboptimal. As

an alternative, the first LHCb measurement [67] made a simultaneous analysis of  $B^\pm \rightarrow DK^\pm$  and a much larger sample of  $B^\pm \rightarrow D\pi^\pm$  decays; since the  $F_i$  parameters relate to the  $D$  decay, they can effectively be obtained in the  $D\pi^\pm$  sample and shared between the two  $B^\pm \rightarrow Dh^\pm$  channels. However, there is  $CP$  violation present in the  $B^\pm \rightarrow D\pi^\pm$  decays, which led to a dominant systematic uncertainty. Later LHCb measurements [3, 73] instead relied on flavour tagged  $D$  mesons from  $\bar{B}^0 \rightarrow D^{*+}(\rightarrow D^0\pi^+)\mu^-\bar{\nu}_\mu X$  decays to obtain  $F_i$ , where no  $CP$  violation is possible. However, due to necessarily different triggering paths and selections, the acceptance profile is not exactly identical between semi-leptonic decays and the  $B^\pm \rightarrow Dh^\pm$  decays of interest. An efficiency correction based on simulation was therefore applied to obtain the correct  $F_i$ , and in this case, the uncertainty related to the correction constituted the largest systematic uncertainty on the measurement.

Both sources of systematic uncertainty can be avoided by making a simultaneous analysis of  $B^\pm \rightarrow DK^\pm$  and  $B^\pm \rightarrow D\pi^\pm$  decays, where  $CP$ -violating observables are measured in *both* channels and the  $F_i$  parameters are shared. Effectively, the  $F_i$  are determined in the high statistics  $B^\pm \rightarrow D\pi^\pm$  channel, but with no systematic effect from  $CP$ -violation in that channel, since the  $CP$ -violation is incorporated in the yield description. At the start of the work that lead to this thesis, it was not clear to what degree the measured  $CP$ -violating observables in  $B^\pm \rightarrow D\pi^\pm$  decays were affected by  $CP$  violation in the neutral kaon sector. The impact had been shown to scale as  $\mathcal{O}(|\epsilon|/r_B)$  [74], which is negligible for the  $B^\pm \rightarrow DK^\pm$  channel but suggests potentially large biases in the  $B^\pm \rightarrow D\pi^\pm$  channel, where  $r_B$  is 20 times smaller. However, the dedicated analysis presented in Chapter 3 has proved the effect on GGSZ measurements to be in fact be *smaller* than  $\mathcal{O}(|\epsilon|/r_B)$  and the simultaneous measurement is indeed viable.

The measurement is performed by making extended maximum-likelihood fits to the  $m_B$  spectra of  $B \rightarrow D(\rightarrow K_S^0 h^+ h^-)h'^\pm$  candidates split by charge and Dalitz bin. The  $B^\pm \rightarrow DK^\pm$  signal yields are parameterised using the expressions in Eq. (1.41) directly, thus obtaining values for  $x_\pm^{DK}$  and  $y_\pm^{DK}$  directly. The Cartesian  $CP$ -violating observables  $x_\pm$  and  $y_\pm$  are employed because they lead to better statistical behaviour than fits to data where the underlying parameters  $(\gamma, r_B^{DK^\pm}, \delta_B^{DK^\pm})$  are determined [], at the cost of introducing a fourth degree of freedom. With the addition of the  $B^\pm \rightarrow D\pi^\pm$  mode as a true signal channel, two new underlying parameters are introduced,  $r_B^{D\pi^\pm}$  and  $\delta_B^{D\pi^\pm}$ . It is only necessary to introduce an additional two, not four, Cartesian parameters [75] by defining

$$\xi_{D\pi^\pm} = \left( \frac{r_B^{D\pi^\pm}}{r_B^{DK^\pm}} \right) \exp[i(\delta_B^{D\pi^\pm} - \delta_B^{DK^\pm})] \quad (1.44a)$$

653 and letting

$$x_\xi^{D\pi} = \text{Re}[\xi_{D\pi^\pm}] \quad y_\xi^{D\pi} = \text{Im}[\xi_{D\pi^\pm}]. \quad (1.44b)$$

654 In terms of these parameters, the usual Cartesian  $x_\pm$  and  $y_\pm$  are given by

$$x_\pm^{D\pi} = x_\xi^{D\pi} x_\pm^{DK} - y_\xi^{D\pi} y_\pm^{DK}, \quad y_\pm^{D\pi} = x_\xi^{D\pi} y_\pm^{DK} + y_\xi^{D\pi} x_\pm^{DK}. \quad (1.45)$$

655 Using this expression, the  $B^\pm \rightarrow D\pi^\pm$  yields can also be defined via Eq. (1.41) in the  
 656 maximum-likelihood fit. This allows for a stable fit for all six  $x$  and  $y$  parameters, as  
 657 well as the shared  $F_i$ , as described in much greater detail in Chapter 4. Note that  $\xi$   
 658 does not depend on  $\gamma$ : all information on  $CP$  asymmetries in both the  $B^\pm \rightarrow DK^\pm$   
 659 and  $B^\pm \rightarrow D\pi^\pm$  channels is encoded in  $x_\pm^{DK}$  and  $y_\pm^{DK}$ .

660 The combined analysis of  $B^\pm \rightarrow DK^\pm$  and  $B^\pm \rightarrow D\pi^\pm$  decays presents a sig-  
 661 nificant step forward, because it solves the problem of obtaining  $F_i$  parameters  
 662 for the appropriate acceptance profile in a manner that avoids leading systematic  
 663 uncertainties, and almost all reliance on simulation. This is of great importance,  
 664 if the large data samples that will be collected by LHCb in the future are to be  
 665 exploited to their full potential.

# 2

666

667

## The LHCb experiment

668 We have a detector? I thought ntuples were made of magic.

### 669 **2.1 Subdetectors**

#### 670 **2.1.1 The VELO**

#### 671 **2.1.2 Magnet and tracking stations**

#### 672 **2.1.3 The RICH**

#### 673 **2.1.4 Calorimeters**

#### 674 **2.1.5 Muon detectors**

### 675 **2.2 Track reconstruction**

### 676 **2.3 The LHCb triggering system**

#### 677 **2.3.1 The level-0 hardware trigger**

#### 678 **2.3.2 High-level triggers**

#### 679 **2.3.3 Offline data filtering: the LHCb stripping**

### 680 **2.4 Simulation**

# 3

681

682

683

## Neutral kaon $CP$ violation and material interaction in BPGGSZ measurements

684 The presence of a  $K_S^0$  meson in the  $D \rightarrow K_S^0 h^+ h^-$  final states introduces a small  
685 bias in BPGGSZ measurements due to  $CP$ -violation in the neutral kaon sector  
686 and asymmetries caused by the interaction between the neutral kaons and detector  
687 material. These fundamental physics effects are reviewed in Section 3.1, after which  
688 the chapter presents a detailed analysis of the impact on the LHCb measurement  
689 that is the subject of the thesis, as well as future  $\gamma$  measurements with the Belle II  
690 experiment. Prior to this analysis, the only existing work on the effect on  $\gamma$   
691 measurements suggested a small effect in  $B^\pm \rightarrow D K^\pm$  measurements but potentially  
692 very significant effects in measurements based on  $B^\pm \rightarrow D \pi^\pm$  decays [74]. However,  
693 as described in Section 3.1.1, the analysis in Ref. [74] does not take into account  
694 the fundamental aspect of the BPGGSZ method: that it relies on the phase-space  
695 distribution of signal decays, not phase-space integrated asymmetries. Furthermore,  
696 the study only considers the  $CP$ -violation effect, not material interaction. Therefore,  
697 a more detailed study was necessary before the  $B^\pm \rightarrow D \pi^\pm$  decay mode could  
698 reliably be promoted to a signal channel.

699

700

### 3.1 $CP$ violation and material interaction of neutral kaons

701 A brief review of the general phenomenology of mixing and  $CP$  violation in the  
702 neutral kaon system is useful, before analysing the impact on  $\gamma$  measurements.

703 The presentation in this section follows the PDG review of  *$CP$  violation in the*  
704 *quark section* [76]. The general theory considers any pair of neutral mesons  $|M^0\rangle$   
705 and  $|\bar{M}^0\rangle$  related by  $CP$  conjugation

$$CP|M^0\rangle = e^{i\phi_M}|M^0\rangle \quad CP|\bar{M}^0\rangle = e^{-i\phi_M}|\bar{M}^0\rangle, \quad (3.1a)$$

706 where  $\phi_M$  is an arbitrary phase. In this thesis, the convention  $\phi_M = 0$  is chosen  
707 to equal zero, so that

$$CP|M^0\rangle = |\bar{M}^0\rangle \quad CP|\bar{M}^0\rangle = |M^0\rangle. \quad (3.1b)$$

708 A meson state that starts as a general superposition of  $|M^0\rangle$  and  $|\bar{M}^0\rangle$  states

$$\begin{aligned} \psi_M^0 &\equiv \psi_M(0) = a(0)|M^0\rangle + b(0)|\bar{M}^0\rangle \\ &\equiv \psi_{M^0}^0 + \psi_{\bar{M}^0}^0 \end{aligned} \quad (3.2)$$

709 will, over time, involve into a state that consists of a different superposition of  
710  $|M^0\rangle$  and  $|\bar{M}^0\rangle$ , as well as components for all possible states the meson system  
711 can decay into

$$\begin{aligned} \psi_M(t) &= a(t)|M^0\rangle + b(t)|\bar{M}^0\rangle + \sum c_i(t)f_i \\ &\equiv \psi_{M^0}(t) + \psi_{\bar{M}^0}(t) + \sum c_i(t)f_i. \end{aligned} \quad (3.3)$$

712 For time scales that are longer than the typical strong-interaction, the time evolution  
713 of the  $M^0 - \bar{M}^0$  superposition can be described by a  $2 \times 2$  Hamiltonian

$$\frac{d}{dt} \begin{pmatrix} \psi_{M^0}(t) \\ \psi_{\bar{M}^0}(t) \end{pmatrix} = -i\mathcal{H}_0 \begin{pmatrix} \psi_{M^0}(t) \\ \psi_{\bar{M}^0}(t) \end{pmatrix} \quad (3.4)$$

714 that is *non-Hermitian* (to allow for decay) but can be parameterised in terms  
715 of two Hermitian matrices  $\mathcal{M}$  and  $\Gamma_0$

$$\mathcal{H}_0 = \mathcal{M} - \frac{i}{2}\Gamma_0. \quad (3.5)$$

716 The quantum states with well-defined (real) masses,  $m_j$ , and (real) decay widths,  
717  $\Gamma_j$ , are the two eigenstates of  $\mathcal{H}_0$  with eigenvalues  $\lambda_j = m_j - \frac{i}{2}\Gamma_j$ . The eigenstates  
718 (of course) evolve independently in time, so that

$$\psi_j(t) = e^{-i\lambda_j t}\psi_j^0 = e^{-im_j t - \frac{\Gamma_j}{2}t}\psi_j^0. \quad (3.6)$$

719 The eigenstates are denoted  $H$  and  $L$  according to the size of  $m_j$ , the real part  
720 of the eigenvalues, such that  $m_H > m_L$ . Assuming that  $\mathcal{H}_0$  conserves  $CPT$  the  
721 eigenstates have the general form

$$\begin{aligned} |M_H\rangle &\equiv p|M^0\rangle - q|\bar{M}^0\rangle \\ |M_L\rangle &\equiv p|M^0\rangle + q|\bar{M}^0\rangle \end{aligned} \quad (3.7)$$

where  $p$  and  $q$  are complex numbers that satisfy  $|q|^2 + |p|^2 = 1$ . With the convention in Eq. (3.1b) it follows that if  $\mathcal{H}_0$  also conserves  $CP$ , so that  $|M_H\rangle$  and  $|M_L\rangle$  are  $CP$  eigenstates, then  $p = \pm q$ , where the sign depends on which of the heavy and the light meson states is  $CP$  even, and which is  $CP$  odd.

The eigenstates of the Hamiltonian governing the neutral kaon system are almost, but not exactly, equal to the  $CP$  eigenstates

$$|K_1\rangle = \frac{|K^0\rangle + |\bar{K}^0\rangle}{\sqrt{2}} \quad |K_2\rangle = \frac{|K^0\rangle - |\bar{K}^0\rangle}{\sqrt{2}}, \quad (3.8)$$

which are  $CP$  even and odd, respectively. This approximate equality leads to the most prominent feature of the neutral kaon system: the two eigenstates of  $\mathcal{H}_0$  have lifetimes that differ by orders of magnitude. This is best understood by assuming, for a moment, that the states in Eq. (3.8) *do* equal the eigenstates with definite life times. The  $K_1$  state can decay in the  $CP$  even  $\pi^+\pi^-$  and  $\pi^0\pi^0$  modes, and does so almost 100% of the time; these decay modes are not available to the  $K_2$  (in the absence of direct  $CP$  violation) which results in a much lower decay rate and much longer life time. Therefore, the eigenstates in the kaon system are labelled the *short-lived* kaon,  $K_S^0$ , which is almost  $CP$  even, and the *long-lived* kaon,  $K_L^0$ , which is almost  $CP$  odd. The life times are [76]

$$\tau_{K_S^0} = (8.954 \pm 0.004) \times 10^{-11} \text{s} \quad \tau_{K_L^0} = (5.116 \pm 0.021) \times 10^{-8} \text{s}. \quad (3.9)$$

Experimentally, it is found that the  $K_S^0$  corresponds to the light eigenstate, but that the mass splitting [76]

$$\begin{aligned} \Delta m = m_{K_L^0} - m_{K_S^0} &= (0.5289 \pm 0.0009) \times 10^{10} \hbar s^{-1} \\ &\simeq 3.5 \times 10^{-6} \text{ eV} \end{aligned} \quad (3.10)$$

is tiny compared to the neutral kaon masses of  $m_{K_S^0} = 497.6 \text{ MeV}/c^2$  [76].

However, the discovery of  $K_L^0 \rightarrow \pi\pi$  decays by Kronin and Fitch in 1964 established that the  $K_S^0$  and  $K_L^0$  are *not* exactly equal to the  $CP$  eigenstates in Eq. (3.8), because the  $\mathcal{H}_0$  relevant to the kaon system is  $CP$ -violating. The  $CP$  violation in the kaon sector is conventionally parameterised in terms of the complex parameters  $\epsilon$  and  $\epsilon'$ , in terms of which

$$\frac{A(K_L^0 \rightarrow \pi^+\pi^-)}{A(K_S^0 \rightarrow \pi^+\pi^-)} = \epsilon + \epsilon' \quad \frac{A(K_L^0 \rightarrow \pi^0\pi^0)}{A(K_S^0 \rightarrow \pi^0\pi^0)} = \epsilon - 2\epsilon'. \quad (3.11)$$

In these expressions  $\epsilon$  denotes the contribution from  $CP$  violation in mixing and  $\epsilon'$  the contribution due to direct  $CP$  violation in the decays. The  $\epsilon$  parameter has been measured to be [76]

$$|\epsilon| = (2.228 \pm 0.011) \times 10^{-3}, \quad \arg \epsilon = (43.52 \pm 0.05)^\circ. \quad (3.12)$$



749 Direct  $CP$  violation is ignored for the remainder of the thesis, because  $\epsilon'$  is measured  
750 to be three orders of magnitude smaller than  $\epsilon$ . In terms of the  $CP$  eigenstates  
751 of Eq. (3.8), the mass eigenstates  $K_S^0$  and  $K_L^0$  are given by

$$\begin{aligned} |K_S^0\rangle &= \frac{|K_1\rangle + \epsilon|K_2\rangle}{\sqrt{1+|\epsilon|^2}} &= \frac{(1+\epsilon)|K^0\rangle + (1-\epsilon)|\bar{K}^0\rangle}{\sqrt{2(1+|\epsilon|^2)}} \\ |K_L^0\rangle &= \frac{|K_2\rangle + \epsilon|K_1\rangle}{\sqrt{1+|\epsilon|^2}} &= \frac{(1+\epsilon)|K^0\rangle - (1-\epsilon)|\bar{K}^0\rangle}{\sqrt{2(1+|\epsilon|^2)}}, \end{aligned} \quad (3.13)$$

752 corresponding to the definition  $p = (1+\epsilon)/\sqrt{2(1+|\epsilon|^2)}$  and  $q = (1-\epsilon)/\sqrt{2(1+|\epsilon|^2)}$   
753 in Eq. (3.7).

754 In an experimental setting, the time evolution of a neutral kaon state is affected  
755 by nuclear interactions with the detector. The interaction is governed by the strong  
756 force, and therefore sensitive to the *flavour* of the kaon state; the interaction  
757 strength is thus different for  $K^0$  and  $\bar{K}^0$  mesons. This difference introduces a  
758 non-zero  $K_S^0 \leftrightarrow K_L^0$  transition amplitude for neutral kaons traversing a detector  
759 segment. This effect was predicted early in the history of kaon physics [77] and is  
760 commonly denoted *kaon regeneration*. The effect can be described by including a  
761 material-interaction term in the Hamiltonian that is diagonal in the  $(|K^0\rangle, |\bar{K}^0\rangle)$   
762 basis, so that the equation governing the time evolution is [78, 79]

$$\frac{d}{dt} \begin{pmatrix} \psi_{K^0}(t) \\ \psi_{\bar{K}^0}(t) \end{pmatrix} = -i \left[ \mathcal{H}_0 + \begin{pmatrix} \chi & 0 \\ 0 & \bar{\chi} \end{pmatrix} \right] \begin{pmatrix} \psi_{K^0}(t) \\ \psi_{\bar{K}^0}(t) \end{pmatrix}. \quad (3.14)$$

763 The complex parameters  $\chi$  and  $\bar{\chi}$  describe the material interaction of the  $K^0$   
764 and  $\bar{K}^0$  flavour eigenstates and are related to their scattering cross section, as  
765 described further in Section 3.3.4. The solution of Eq. (3.14) for the time evolution  
766 in the  $K_S^0$  and  $K_L^0$  states is [79]

$$\begin{aligned} \psi_S(t) &= e^{-i\Sigma t} \left( \psi_S^0 \cos \Omega t + \frac{i}{2\Omega} (\Delta\lambda\psi_S^0 - \Delta\chi\psi_L^0) \sin \Omega t \right), \\ \psi_L(t) &= e^{-i\Sigma t} \left( \psi_L^0 \cos \Omega t - \frac{i}{2\Omega} (\Delta\lambda\psi_L^0 + \Delta\chi\psi_S^0) \sin \Omega t \right), \end{aligned} \quad (3.15)$$

767 in terms of the parameters

$$\begin{aligned} \Delta\chi &= \chi - \bar{\chi}, \\ \Delta\lambda &= \lambda_L - \lambda_S = (m_L - m_S) - \frac{i}{2}(\Gamma_L - \Gamma_S), \\ \Sigma &= \frac{1}{2}(\lambda_S + \lambda_L + \chi + \bar{\chi}), \\ \Omega &= \frac{1}{2}\sqrt{\Delta\lambda^2 + \Delta\chi^2}. \end{aligned} \quad (3.16)$$

768 In the vacuum limit where  $\chi = \bar{\chi} = 0$ , the expressions in Eq. (3.6) and Eq. (3.15) are  
769 equal.

### 3.1.1 A first look at the impact on $\gamma$ measurements

The effects described above have an impact on measurements of  $CP$  asymmetries in modes with a neutral kaon in the final state. This was analysed for the first time in relation to  $\gamma$  measurements by Grossman and Savastio in 2014 [74]. The authors point out two sources of corrections to be included:

- the fact that  $K_S^0$  is not an exact  $CP$  eigenstate can break potential symmetry relations employed in an analysis, and
- that when the neutral kaon is reconstructed in a  $\pi\pi$  final state there will be contributions from both  $K_S^0$  and  $K_L^0$  decays.

The analysis in this chapter considers yet another effect, not treated by Grossman and Savastio, namely that

- material interaction can emulate the effect of neutral kaon  $CP$  violation, because it couples the almost- $CP$ -even  $K_S^0$  and the almost- $CP$ -odd  $K_L^0$  states.

Due to the presence of  $K_L^0 \rightarrow \pi\pi$  decays, Grossman and Savastio point out that the relevant decay rates to consider in an experimental setting are of the form

$$d\Gamma(t) \propto |\psi_S(t) + \epsilon\psi_L(t)|^2. \quad (3.17)$$

The time dependence of the decay rates considered in Chapter 1 was left out because all terms shared a common time dependence. That is not the case in Eq. (3.17), due to the very different decay rates of the  $K_S^0$  and  $K_L^0$  components of the kaon state. As a consequence, the time-integrated yields have the form

$$N \propto \int dt \eta(t) |\psi_S(t) + \epsilon\psi_L(t)|^2, \quad (3.18)$$

where  $\eta(t)$  is the time acceptance in a given experimental setting. Thus, the acceptance is crucial to model in order to correctly estimate the impact of kaon  $CP$ -violation effects on a given measurement.

Considering BPGBSZ measurements, the main effect of neutral kaon  $CP$  violation is a breakdown of the fundamental Dalitz-plot symmetry that is exploited in the derivation of the bin yield equations. Extending the amplitude definition of Eq. (1.21) to include  $K_L^0$  decays

$$A_{S(L)}^{(\overline{D})}(s_-, s_+) = A((\overline{D})^0 \rightarrow K_{S(L)}^0 \pi^+ \pi^-), \quad (3.19)$$

the authors point out that  $CP$ -violation in the  $K_S^0$  system means that the relation  $A_S^{(\overline{D})}(s_{-+}) = A_S^D(s_{+-})$  is not exactly true; and in addition, there is now a

dependence on  $A_L^D(s_{-+})$  which satisfies a different approximate symmetry, namely  $A_L^{\bar{D}}(s_{-+}) \simeq -A_L^D(s_{+-})$ . Grossman and Savastio describe these symmetry breaking effects in detail, but do not explicitly derive the corrections to the yield equations of Chapter 1, nor try to quantify the potential bias on  $\gamma$  in a measurement based on the binned yields. Instead, they derive expressions for the bias in a measurement obtained from phase-space integrated  $CP$  asymmetries. This is done for both GLW measurements that use  $D \rightarrow K_S^0 X$  final states and for the  $D \rightarrow K_S^0 h^+ h^-$  final states; however, for their quantitative estimate of  $\Delta\gamma$  the authors make an approximation that corresponds to assuming that the  $D \rightarrow K_S^0 h^+ h^-$  final state is a  $CP$  eigenstate, making the two results identical. The authors find that in this case, assuming a uniform experimental acceptance for all kaon decay times, the asymmetry has the form<sup>1</sup>

$$A = \frac{2r_B \sin \gamma \sin \delta_B + 2\text{Re}[\epsilon]}{1 + r_B^2 - 2r_B \cos \gamma \cos \delta_B}, \quad (3.20)$$

If a measured value of  $A$  is interpreted to obtain  $\gamma$  without taking the  $\epsilon$  term into account, it leads to a bias of

$$\Delta\gamma = -\frac{\text{Re}[\epsilon]}{r_B \cos \gamma \sin \delta_B} + O(|\epsilon|). \quad (3.21)$$

The scaling  $\Delta\gamma \sim \mathcal{O}(r_B/|\epsilon|)$  is the main result of the analysis by Grossman and Savastio. For  $B^\pm \rightarrow D K^\pm$  decays, where  $r_B^{DK^\pm} \simeq 0.1$  this suggests a bias at the percent level, which is negligible compared to current experimental uncertainties. However, in the  $B^\pm \rightarrow D \pi^\pm$  case, where  $r_B^{D\pi^\pm} \simeq 0.005$  [47], their result suggests relative biases that are potentially of  $\mathcal{O}(1)$ .

The conclusions are lacking on two accounts, however. Firstly, as made clear in Section 1.3.5, the  $K_S^0 \pi^+ \pi^-$  and  $K_S^0 K^+ K^-$  states are *far from*  $CP$  eigenstates. From the asymmetry expression in that section, it is clear that the bias in a determination of  $\gamma$  based on phase-space asymmetries will in fact scale as

$$\Delta\gamma \sim \mathcal{O}\left(\frac{|\epsilon|}{(2\mathcal{F}_+ - 1)r_B}\right), \quad \boxed{\phantom{000}} \quad (3.22)$$

which suggests that Grossman and Savastio severely *underestimates* the potential impact. This is described in detail in Section 3.2.3. More importantly, the analysis of the phase-space integrated asymmetry is in fact *irrelevant* to BPGGSZ measurements as they are currently performed: as described in Section 1.3.5 the information from

---

<sup>1</sup>In fact the expression in Eq. (3.20) is missing a term, as will be clear when an analogous expression is derived in detail in Section 3.2.3.

the global asymmetry is completely discarded. Therefore it is necessary to analyse the effects of kaon  $CP$ -violation on a full, binned analysis of  $D \rightarrow K_S^0 h^+ h^-$  decays, which is done in detail in the following sections. While the aim is to extend the analysis if Grossman and Savastio, the treatment in the following sections is completely independent of that in Ref. [74].

## 3.2 Impact on BPGBSZ measurements of $\gamma$ : principles

The analysis of the impact on BPGBSZ measurements is carried out in two stages. This section treats the leading order effects analytically, and derives the overall order of magnitude of the expected bias in a general setting. Then Section 3.3 presents a detailed numerical study of the expected effect in measurements with the LHCb and Belle II experiments specifically, because these will be crucial to constrain  $\gamma$  during the coming decade [80, 81].

### 3.2.1 Modified symmetry relations

In order to derive the corrections to the asymmetry relation  $A_S^D(s_{-+}) \simeq A_S^{\bar{D}}(s_{+-})$ , it is beneficial to express  $A_{S(L)}^D$  in terms of the amplitudes

$$A_{1/2}^{\bar{D}} = A(\bar{D}^0 \rightarrow K_{1/2}^0 \pi^+ \pi^-), \quad (3.23)$$

because these amplitude satisfy the exact symmetries  $A_1^D(s_{-+}) = A_1^{\bar{D}}(s_{+-})$  and  $A_2^D(s_{-+}) = -A_2^{\bar{D}}(s_{+-})$ . This approach is different to that of Grossman and Savastio, but the final results are equivalent. After the decay of a  $D^0$  meson to a neutral kaon, the kaon state is

$$\begin{aligned} \psi^0 &= A_1^D |K_1\rangle + A_2^D |K_2\rangle \\ &= N \left[ (A_1^D - \epsilon A_2^D) |K_S^0\rangle + (A_2^D - \epsilon A_1^D) |K_L^0\rangle \right], \end{aligned} \quad (3.24)$$

with the normalisation constant  $N = \sqrt{1 + |\epsilon|^2}/(1 - \epsilon^2)$ . Thus it can be seen that

$$\begin{aligned} A_S^D(s_{-+}) &= N \left[ (A_1^D(s_{-+}) - \epsilon A_2^D(s_{-+})) \right], \\ A_L^D(s_{-+}) &= N \left[ (A_2^D(s_{-+}) - \epsilon A_1^D(s_{-+})) \right], \end{aligned} \quad (3.25)$$

with an analogous expression for the  $\bar{D}^0$  decay amplitudes. Therefore, the generalised relations between the  $D^0$  and  $\bar{D}^0$  amplitudes are

$$\begin{aligned} A_S^{\bar{D}}(s_{+-}) &= N[A_1^{\bar{D}}(s_{+-}) - \epsilon A_2^{\bar{D}}(s_{+-})] \\ &= N[A_1^D(s_{-+}) + \epsilon A_2^D(s_{-+})] = A_S^D(s_{-+}) + 2N\epsilon A_2^D(s_{-+}), \\ A_L^{\bar{D}}(s_{+-}) &= N[A_2^{\bar{D}}(s_{+-}) - \epsilon A_1^{\bar{D}}(s_{+-})] \\ &= -N[A_2^D(s_{-+}) + \epsilon A_1^D(s_{-+})] = -A_L^D(s_{-+}) - 2N\epsilon A_1^D(s_{-+}). \end{aligned} \quad (3.26)$$

### 3.2.2 Relationship between the $K_S^0$ and $K_L^0$ amplitudes

The decay amplitude  $A(D^0 \rightarrow K_S^0 \pi^+ \pi^-)$  has been carefully studied, and a number of amplitude models have been published [51, 56–58, 61]. No models have been published for  $D^0 \rightarrow K_L^0 \pi^+ \pi^-$  decays. However, following an approach laid out by the CLEO collaboration [69], the two amplitudes can be related. Again, this is most easily done by relating the  $A_1^D(s_{+-})$  and  $A_2^D(s_{+-})$  amplitudes. In the isobar formalism, the decay amplitude  $A(D^0 \rightarrow K_1 \pi^+ \pi^-)$  is expressed as a non-resonant constant amplitude plus a sum of resonances

$$A(D^0 \rightarrow K_1 \pi^+ \pi^-) = k_{NR} + \sum_{CF} k_i R^i(s_{K\pi^-}) + \sum_{DCS} k_j R^j(s_{K\pi^+}) + \sum_{R_{\pi\pi}} k_k R^k(s_{\pi^+\pi^-}). \quad (3.27)$$

The resonances are split into Cabibbo-favoured (CF)  $K^{*-}$  resonances, doubly Cabibbo-suppressed (DCS)  $K^{*+}$  resonances and  $\pi\pi$  resonances.<sup>2</sup> The CF resonances couple to the  $\bar{K}^0$  component of  $K_1 (\propto K^0 + \bar{K}^0)$ , and therefore the corresponding  $k_i$  in the  $K_2 (\propto K^0 - \bar{K}^0)$  amplitude will have a relative minus sign. The DCS resonances couple to the  $K^0$  component of  $K_1$ , and so the corresponding  $k_j$  in the  $K_2$  amplitude will have a relative plus sign. For the  $h^+ h^-$  resonances, there will be a coupling to both the  $K^0$  and  $\bar{K}^0$  components, however the coupling to the  $K^0$  component is expected to be suppressed with a Cabibbo suppression factor  $r_k e^{i\delta_k}$ , where  $r_k \simeq \tan^2 \theta_C \simeq 0.05$  is determined by the Cabibbo angle  $\theta_C$  and  $\delta_k$  can take any value. Therefore, the  $k_k$  for these resonances have a relative  $-(1 - 2r_k e^{i\delta_k})$  factor in the  $K_2$  amplitude. The same effect leads to the differences in decay rates between  $D^0 \rightarrow K_S^0 \pi^0$  and  $D^0 \rightarrow K_L^0 \pi^0$  decays [82, 83]. Thus, given a model of the

---

<sup>2</sup>In modern models, the  $\pi\pi$  and  $K\pi$   $S$ -wave components are modelled via the  $K$ -matrix formalism and LASS parametrisations, respectively, instead of sums of individual resonances [51]. This does not alter the arguments below, as the  $R$  functions of Eq. (3.27) can equally well represent such terms.

form in Eq. (3.27), a model for the  $A(D^0 \rightarrow K_2\pi^+\pi^-)$  amplitude will have the form

$$A(D^0 \rightarrow K_2\pi^+\pi^-) = k_{NR} + \sum_{CF} (-k_i) R^i(s_{K\pi^-}) + \sum_{DCS} (+k_j) R^j(s_{K\pi^+}) + \sum_{R_{\pi\pi}} (-(1 - 2r_k e^{i\delta_k}) k_k) R^k(s_{\pi^+\pi^-}). \quad (3.28)$$

An important consequence of these substitution rules is that

$$A_2^D(s_{+-}) = -A_1^D(s_{+-}) + r_A \Delta A(s_{+-}), \quad (3.29)$$

where  $r_A \simeq \tan^2 \theta_C$  and  $\Delta A(s_{+-}) \sim A_1^D(s_{+-})$  are of the same order of magnitude (at least when averaged over the bins used in  $\gamma$  measurements). This relation is sufficient to make the qualitative arguments of this section, while the full set of substitution rules above are used in the quantitative studies of Section 3.3.

### 3.2.3 Modification of the BPGBSZ yield equations

With suitable models to calculate  $A_{S(L)}^{\bar{D}}$  (or  $A_{1/2}^{\bar{D}}$ ) and knowledge of  $\Delta\chi$  for the materials relevant to an experimental setting, the relations derived in the preceding sections can be employed to calculate the expected phase-space bin yields,  $N_i^\pm$ , including the effects of kaon  $CP$  violation and material interaction. The decay rates have additional terms compared to those in Eq. (1.24), because the  $K_L^0$  contribution must be taken into account

$$d\Gamma(t, s_{+-}) \propto |\psi_S(t, s_{+-}) + \epsilon\psi_L(t, s_{+-})|^2, \quad (3.30)$$

where the time-dependence of  $\psi_{S/L}(t, s_{+-})$  is governed by Eq. (3.15), and the phase-space dependence is included in the state component, by defining  $\psi_{S/L}^0$  in terms of  $A_{S(L)}^{\bar{D}}(s_{+-})$ . For example, for the case of a  $B^- \rightarrow DK^-$  decay, the definition is

$$\begin{aligned} \psi_{S/L}^{0,B^-}(s_{+-}) &= A_S^D(s_{+-}) + r_B e^{i(\delta_B - \gamma)} A_S^{\bar{D}}(s_{+-}) \\ &= A_1^D(s_{+-}) - \epsilon A_2^D(s_{+-}) + r_B e^{i(\delta_B - \gamma)} (A_1^{\bar{D}}(s_{+-}) - \epsilon A_2^{\bar{D}}(s_{+-})) \\ &= A_1^D(s_{+-}) - \epsilon A_2^D(s_{+-}) + r_B e^{i(\delta_B - \gamma)} (A_1^D(s_{+-}) + \epsilon A_2^D(s_{+-})). \end{aligned} \quad (3.31)$$

It is useful to look at the corrections to the BPGBSZ yield expressions in Eq. (1.25) to lowest order in  $\epsilon$  and  $r_\chi = \frac{1}{2} \frac{\Delta\chi}{\Delta\lambda}$ , the dimensionless parameter governing material interactions. For LHCb and Belle II the average  $|r_\chi| \simeq 10^{-3}$ , as detailed in the Section 3.3. To first order in  $r_\chi$ , the time-dependent kaon states within a material, given in Eq. (3.15), simplify to [79]

$$\begin{aligned} \psi_S(t, s_{+-}) &= e^{-\frac{i}{2}(x+\bar{x})t} e^{-i\lambda_{St}} (\psi_S^0(s_{+-}) - r_\chi (1 - e^{-i\Delta\lambda t}) \psi_L^0(s_{+-})), \\ \psi_L(t, s_{+-}) &= e^{-\frac{i}{2}(x+\bar{x})t} e^{-i\lambda_{Lt}} (\psi_L^0(s_{+-}) + r_\chi (1 - e^{+i\Delta\lambda t}) \psi_S^0(s_{+-})). \end{aligned} \quad (3.32)$$

By inserting these expressions into Eq. (3.30) and employing the definition in Eq. (3.31) (and a similar definition for  $B^+$  decays), the binned yields can be calculated by an integration over time and phase space. In the remainder of this section, it is assumed that the experimental time acceptance is  $\eta(t) = 1$  for all times and that  $r_\chi$  is constant at all times; more realistic assumptions are introduced in Section 3.3. In this case, the binned yields are given by the expression

$$\begin{aligned} N_i^- &= h_B^{-'} \left( \hat{K}_{+i} + r_B^2 \hat{K}_{-i} + 2\sqrt{\hat{K}_{+i} \hat{K}_{-i}} (x_- \hat{c}_i + y_- \hat{s}_i) + O(r\epsilon) \right), \\ N_i^+ &= h_B^{+'} \left( \hat{K}_{-i} + r_B^2 \hat{K}_{+i} + 2\sqrt{\hat{K}_{+i} \hat{K}_{-i}} (x_+ \hat{c}_i - y_+ \hat{s}_i) + O(r\epsilon) \right), \end{aligned} \quad (3.33)$$

where a number of new parameters have been defined, and where  $O(r\epsilon)$  denotes terms of  $O(r_A\epsilon)$ ,  $O(r_B\epsilon)$ ,  $O(r_A r_\chi)$ , and  $O(r_B r_\chi)$ . Since  $r_B \sim r_A \sim 10^{-1}$  (in  $B^\pm \rightarrow D K^\pm$  decays) and  $r_\chi \sim \epsilon \sim 10^{-3}$ , these terms are all of the same order of magnitude.

The new normalisation constants  $h_B^{\pm'} = h_B^\pm (1 + |\epsilon + r_\chi|^2 \frac{\Gamma_S}{\Gamma_L} \mp \Delta h)$  are defined in terms of

$$\Delta h = 2\text{Re}[\epsilon + r_\chi] - 4 \frac{\Gamma_S}{\Gamma_L + \Gamma_S} \frac{\text{Re}[\epsilon + r_\chi] + \mu \text{Im}[\epsilon + r_\chi]}{1 + \mu^2}, \quad \mu = 2 \frac{m_L - m_S}{\Gamma_L + \Gamma_S}. \quad (3.34)$$

The  $\hat{K}_i$  parameters are defined to be

$$\hat{K}_i = \frac{1}{1 + |\epsilon + r_\chi|^2 \frac{\Gamma_S}{\Gamma_L}} \left( K_i^{(1)} + |\epsilon + r_\chi|^2 \frac{\Gamma_S}{\Gamma_L} K_i^{(2)} \right), \quad (3.35)$$

in which the  $K_i^{(1/2)}$  parameters are phase-space integrals, defined as in Eq. (1.27) but for  $A_{1/2}^D$ . To lowest order, the  $\hat{K}_i$  correspond to the fractional  $D^0$  decay yield in each bin, as obtained in a measurement that averages  $D^0$  and  $\bar{D}^0$  decays, and assumes the  $A_S^{\bar{D}}(s_{-+}) = A_S^D(s_{+-})$  symmetry to be exact:

$$K_i^{\text{meas}} \equiv \frac{N_i^D + N_{-i}^{\bar{D}}}{\sum_j N_j^D + N_{-j}^{\bar{D}}} = \hat{K}_i + \mathcal{O}(r\epsilon). \quad (3.36)$$

Here,  $N_i^D$  ( $N_i^{\bar{D}}$ ) is the expected yield of flavour tagged  $D^0$  ( $\bar{D}^0$ ) mesons into bin  $i$  of the  $D$  decay phase-space.

In similar fashion, the parameters  $(\hat{c}_i, \hat{s}_i)$  have been introduced to denote the measured average strong-phases, which are expected to differ from  $(c_i, s_i)$  at  $O(\epsilon)$ , since neutral kaon  $CP$  violation is not taken into account in the measurements by CLEO. Thus, any corrections arising if  $(\hat{c}_i, \hat{s}_i)$  and  $(c_i, s_i)$  are substituted in Eq. (3.33) will appear in the  $O(r_B\epsilon)$  terms.

Two observations can be made from the expression in (3.33). The first is that the phase-space distribution is only changed at  $O(r\epsilon)$  compared to the expression in

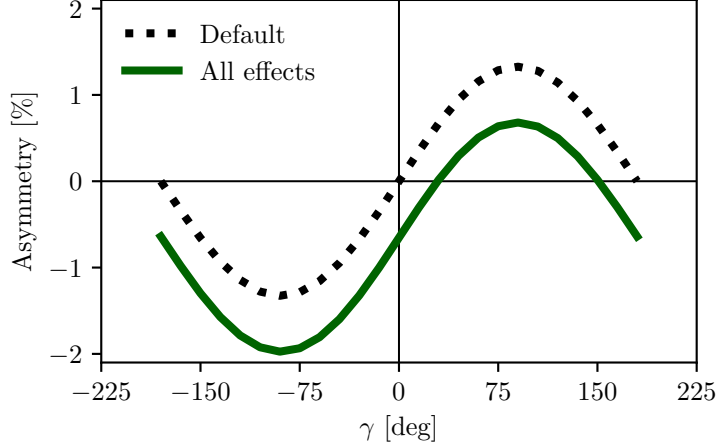


**Figure 3.1:** The asymmetry  $A_{\text{total}}$  as a function of  $\gamma$  calculated to  $O(\epsilon)$  using Eq. (3.37). The calculation is made using for (black dotted line) the default case where  $\Delta h = 0$  and (green) including neutral kaon  $CP$ -violation and material interaction with  $r_\chi = \epsilon$ .

Eq. (1.25), if the measured  $\hat{K}_i$  are used in the experimental analysis. This equally true whether the  $K_i$  are fitted in the signal channel along with  $x_\pm$  and  $y_\pm$ , as is the case in the measurement presented in the thesis, or if they are obtained in a control channel with flavour tagged  $D$  decays, according to Eq. (3.36). As the  $D^0 - \bar{D}^0$  interference term that provides sensitivity to  $\gamma$  enters at order  $O(r_B)$ , the impact on  $\gamma$  measurements can be expected to be  $\Delta\gamma/\gamma \sim O(r\epsilon/r_B)$ . For  $B \rightarrow DK$  analyses, where  $r_B \simeq 0.1$ , this is at the permille level, so the induced  $\Delta\gamma$  bias can be expected to be smaller than  $1^\circ$ . Even in the case of  $B^\pm \rightarrow D\pi^\pm$  decays, this suggests biases that are maximally a few percent. This is the main result of the chapter, because it means that the effect of neutral kaon  $CP$  violation and material interaction is small compared to the precision of the measurement that is the main subject of the thesis.

The second observation relates to potential future measurements of  $\gamma$ , which may also include sensitivity from the total, phase-space-integrated yield asymmetry

$$A_{\text{total}} = \frac{N^- - N^+}{N^- + N^+} = \frac{2(2\mathcal{F}_+ - 1)r_B \sin \delta_B \sin \gamma + \Delta h}{1 + r_B^2 + 2(2\mathcal{F}_+ - 1)r_B \cos \delta_B \cos \gamma} + O(r\epsilon), \quad (3.37)$$

where the definition of  $\mathcal{F}_+$  from Section 1.3.5 has been employed. In the limit  $r_B \rightarrow 0$  the expression agrees with the result for the analogous asymmetry in  $D^\pm \rightarrow \pi^\pm K_S^0$  decays in Ref. [84], evaluated to  $O(\epsilon)$  for an infinite and uniform time-acceptance. As hinted at above, the fact that  $\mathcal{F}_+ \simeq 0.5$  means that the asymmetry due to  $\gamma$  being non-zero is not  $\mathcal{O}(r_B)$ , but of approximately the same order of magnitude as the asymmetry due to  $CP$  violation in the neutral kaon sector, governed by  $\Delta h$ . This is illustrated in Fig. 3.1, where the expression in Eq. (3.37) is plotted in the default

case where  $\Delta h = 0$ , using the model in Ref. [51] to calculate  $K_i$  and  $c_i$ , as well as including neutral kaon  $CP$  violation and material interaction effects, calculated using  $r_\chi = \epsilon$ , with  $\epsilon$  taking the value in Eq. (3.12). The asymmetry changes significantly when including the latter effects. Therefore, measurements based only on the global asymmetry will suffer relative biases of tens of degrees, not a few degrees, if neutral kaon  $CP$  violation and material interaction is not taken into account.

### 3.3 Impact on BPGBGSZ measurements of $\gamma$ : LHCb and Belle II measurements

The previous section has established that the bias due to neutral kaon  $CP$  violation and material interaction is at the sub-percent level for measurements based on  $B^\pm \rightarrow DK^\pm$  decays, and just a few percent in  $B^\pm \rightarrow D\pi^\pm$  decays. Thus, the effects only contribute a manageable systematic uncertainty in the measurement that is the subject of the thesis. However, the expected precision on  $\gamma$  measurements will increase significantly in the coming decade, as both the LHCb [81] and Belle II [80] collaborations expect to make BPGBGSZ measurements that measure  $\gamma$  with a precision of 1–3°. Therefore a deeper understanding of the expected bias for these specific experiments is important.

This section details a study, where the equations of the previous section are evaluated numerically to all orders, and care is taken to realistically model the experiment specific conditions. The scope of the original analysis, published in Ref. [2], was a stand-alone paper that covers both LHCb and Belle II, and which therefore does not rely on full detector simulation. Instead the following approaches are taken to model the necessary input

- the experimental time-acceptance is modelled based on the detector geometry and typical neutral kaon momentum spectrum
- the material interaction is included, using the material budget information available in the technical design reports on each experiment
- both the time-acceptance and material interaction depends on the neutral kaon momentum, for which realistic distributions are estimated using the `RapidSim` simulation package [85].

Each input is described in detail in the following sections. The study has been repeated to assign a systematic uncertainty to the LHCb measurement in Chapter 4, with slight adjustments to match the exact fit setup and with the inputs above extracted from full LHCb simulation. This is described further in Section 3.3.7.

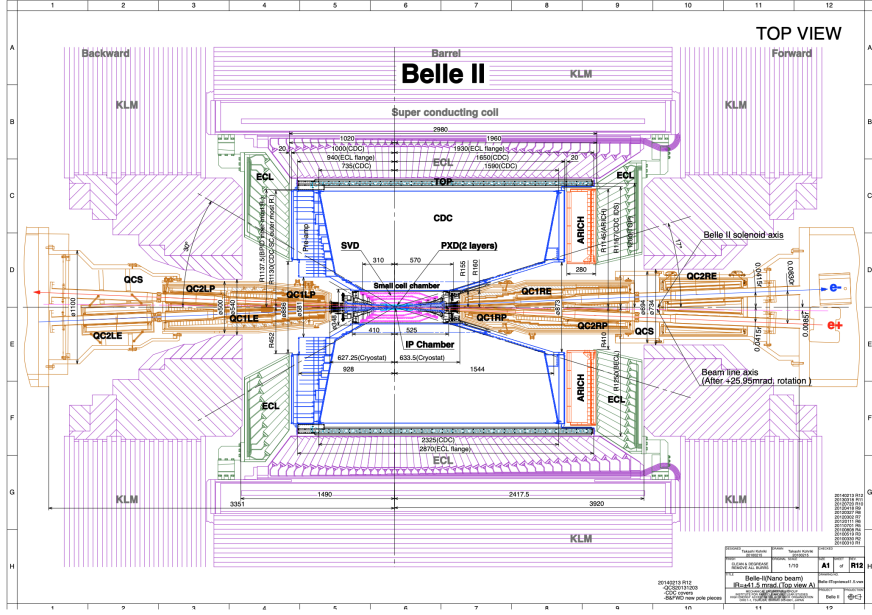


**Figure 3.2:** Schematic of the Belle II detector, reproduced from Ref. [80].

### 3.3.1 Detector geometries

The LHCb geometry and sub detectors are described in details in Chapter 2. In the LHCb measurement discussed in Chapter 4, the  $K_S^0$  mesons are reconstructed in the  $\pi^+\pi^-$  final state and two distinct categories of decay are considered, depending on where in the detector the  $K_S^0$  decay occurs. The categories have very different decay-time acceptance, and therefore two scenarios are considered for LHCb: one in which the decay products of the  $K_S^0$  leave reconstructed tracks in both the silicon vertex detector and downstream tracking detectors (denoted *long-long* or LL), and one in which the decay products of the  $K_S^0$  only leave tracks in the downstream tracking detectors (denoted *down-down* or DD).

The Belle II detector is a general purpose spectrometer, built to collect data from asymmetric  $e^+e^-$  collisions made by the SuperKEKB accelerator in Japan [80]. A schematic of the detector is shown in Fig. 3.2. The relevant sub detectors for the present study are the tracking detectors: a central silicon vertex detector, comprised of a total of six layers within 140 mm of the beam, and a large volume drift chamber with 56 wire layers, extending to a radius of 1130 mm [80]. A single scenario is considered for Belle II, because essentially all the  $K_S^0$  mesons produced in signal decays in Belle II decay within the tracking volume, with more than 90 % decaying in the vertex detector according to the studies described below. Thus, three scenarios are considered in total: LL LHCb, DD LHCb, and Belle II.

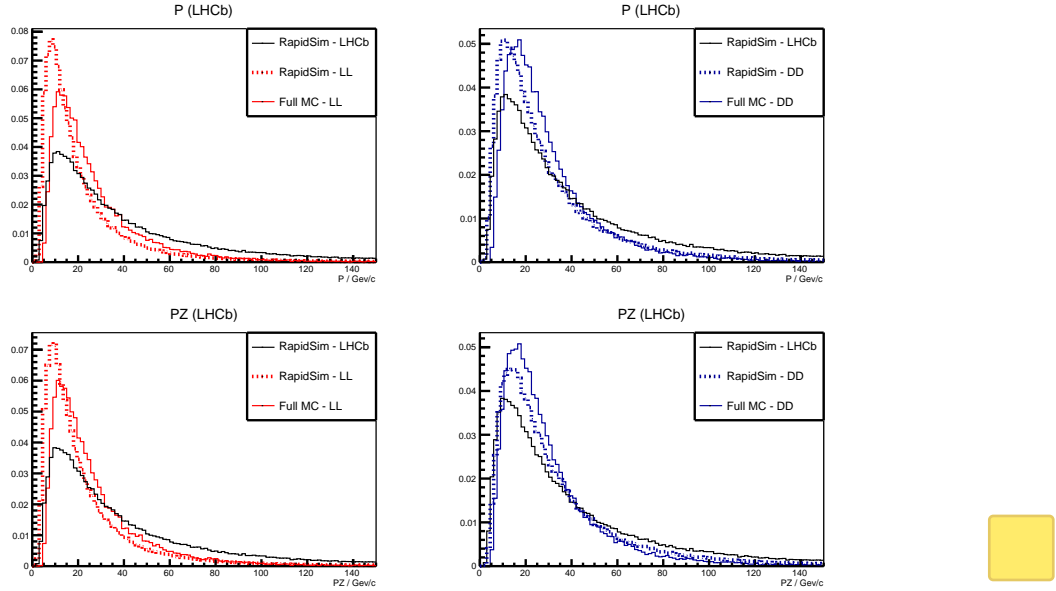


**Figure 3.3:** Momentum spectra for the  $K_S^0$  meson in LHCb, as generated using **RapidSim** (black lines) directly, as well as reweighted to match decay time acceptance in the (red) LL and (blue) DD data categories of LHCb. The LHCb spectra are compared with the spectra in fully simulated signal decays, for both (dotted red lines) LL and (dotted blue lines) DD data categories.

### 3.3.2 Kaon momentum distributions

The neutral kaon momentum distributions are obtained using **RapidSim** [85], a simple tool to generate MC samples. **RapidSim** has an inbuilt capability to generate decays of  $B$  mesons with the kinematic distribution found in LHCb collisions and falling in the LHCb acceptance. However, the distributions need to be reweighted to take the kaon-decay-time acceptance into account. After being reweighted, the **RapidSim** momentum spectra are reasonably close to those found in full LHCb simulation samples of  $B^\pm \rightarrow D(\rightarrow K_S^0\pi^+\pi^-)K^\pm$  decays, as seen in Fig. 3.3

At Belle II, the signal  $B$  mesons stem from decays of  $\Upsilon(4S)$  mesons produced in asymmetric electron-positron collisions. This leads to substantially different decay kinematics in comparison to those found at LHCb. The momentum distribution in Belle II is estimated by letting **RapidSim** decay  $B$  mesons with a momentum of 1.50 GeV/ $c$  along the  $z$ -axis using **RapidSim**, corresponding to the  $\gamma\beta = 0.28$  boost of the centre-of-mass system in Belle II when operated at the  $\Upsilon(4S)$  resonance [80]. A perfect  $4\pi$  angular acceptance is assumed. It is not necessary to reweigh the Belle II momentum spectrum to account for the kaon-decay-time acceptance because all produced  $K_S^0$  mesons decay in the tracking volume.

The resulting momentum distributions for the three types of sample are shown in Fig. 3.4.

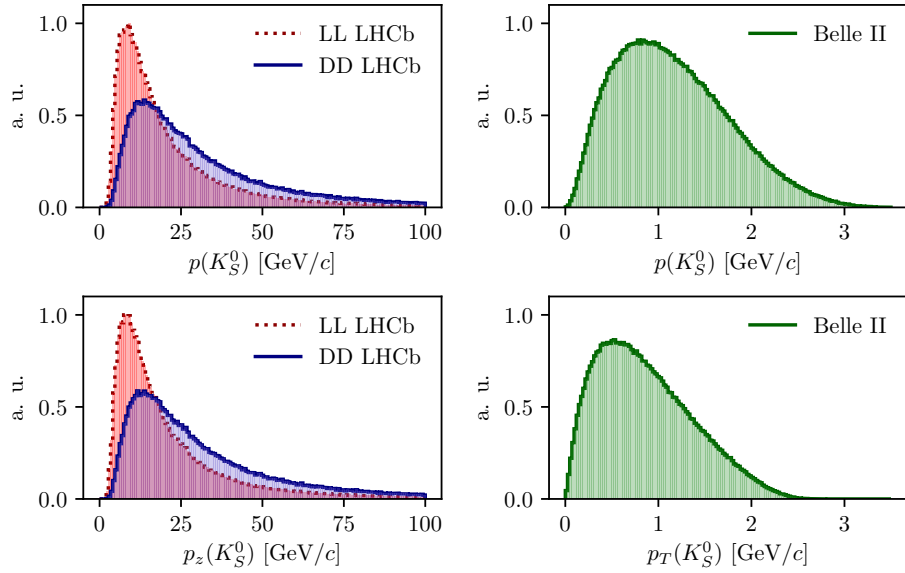


**Figure 3.4:** Momentum distributions for the LHCb (red dotted line) LL and (blue) DD categories, as well as (green) Belle II, obtained using `RapidSim`.

### 3.3.3 Experimental time acceptance

In order to model the experimental time acceptance, the time-dependent decay rates are only integrated over a finite time interval  $(\tau_1, \tau_2)$ . The intervals are defined for each of the three experimental categories, by requiring that a neutral kaon, if produced at  $x = y = z = 0$  with momentum  $p = (p_T, p_z)$ , decays within the relevant part of the corresponding detector. For the LL LHCb category, it is required that the kaon decays before reaching  $z_{max} = 280$  mm, corresponding to a decay where the decay products traverse at least 3 VELO segments (ignoring a number of widely spaced VELO segments placed at a distance of up to  $z = 750$  mm from the interaction point) [86]. For the DD LHCb category a decay at  $z \in [280, 2350]$  mm is required, corresponding to decay between the LL cut-off and the first downstream tracking station [87]. The time acceptance has a significant impact for the LHCb categories, where some 20 % of the kaons escape the tracking stations completely before decaying.

For Belle II, it is assumed that the  $K_S^0$  reconstruction is similar to the Belle  $K_S^0$  reconstruction, which is based on a neural network and reconstructs  $K_S^0$  decays for which the decay product leave tracks in both the drift chamber and silicon vertex detectors, as well as decays that leave tracks in the drift chamber only [88, 89]. Therefore, the  $K_S^0$  decay is required to be within  $r_{max} = 1130$  mm of the beam axis, corresponding to a decay within the outer radius of the drift-chamber. In practice,





1027 most of the kaons decay inside the silicon vertex detector, and requiring a decay  
1028 before 1130 mm is essentially equivalent to having no time cut-off.

### 1029 3.3.4 Detector material budget

1030 The effect of the material interaction is governed by parameter  $\Delta\chi$  of Eq. (3.16). The  
1031 parameter varies along a given kaon path, as the kaon intersects detector components  
1032 made of different materials. In these studies, the calculations are simplified by  
1033 using a single average material parameter for each experimental scenario. The  
1034 average material parameters can be estimated for a given experimental scenario  
1035 by considering the type and length of material traversed by a kaon in the relevant  
1036 sub-detector(s). The average value is estimated, by exploiting that  $\Delta\chi$  is related to  
1037 the forward scattering amplitude  $f$  ( $\bar{f}$ ) of  $K^0$  ( $\bar{K}^0$ ) mesons in a given material [78,79]

$$\Delta\chi = -\frac{2\pi\mathcal{N}}{m_K}(f - \bar{f}) = -\frac{2\pi(N_A\rho/A)}{m_K}(f - \bar{f}), \quad (3.38)$$

1038 where  $\mathcal{N} = N_A\rho/A$  is the scattering centre density of the material,  $m_K$  is the mass  
1039 of the kaon state,  $A$  and  $\rho$  are the nucleon number and density of the material,  
1040 and  $N_A$  is Avogadro's number. Measurements made for a range of nuclei [90] show  
1041 that in the momentum range  $p_K \in [20, 140] \text{ GeV}/c$

$$\left| \frac{f - \bar{f}}{p_K} \right| = 2.23 \frac{A^{0.758}}{p_K^{0.614} (\text{GeV}/c)} \text{ mb}, \quad \arg[f - \bar{f}] = -\frac{\pi}{2} (2 - 0.614), \quad (3.39)$$

1042 where the phase of  $\Delta f$  is determined via a phase-power relation [91]. In the numerical  
1043 studies presented here, Eq. (3.39) is also used for the low momentum neutral kaons  
1044 in the Belle II calculations, as a more detailed modelling of the low momentum  $\Delta\chi$   
1045 based on Ref. [92] is found to yield very similar results. The scattering centre density  
1046  $\mathcal{N}$  is approximated as being constant, equal to the average density along a neutral  
1047 kaon path due to its intersection with different detector segments. This average is  
1048 estimated using the simplifying assumption that the total detector material budget  
1049 is due to silicon. In practice,  $\mathcal{N} = N_A\rho/A$  is calculated using  $A = 28$  and  $\rho = f^{\text{Si}}\rho^{\text{Si}}$ ,  
1050 where  $f^{\text{Si}} < 1$  is the average fraction of a neutral kaon path length that is inside  
1051 detector material, estimated via the known dimensions of the detector, the average  
1052 nuclear interaction length seen by a track traversing it cf. the technical design  
1053 reports [86,93], and the nuclear interaction length of silicon  $\lambda_I^{\text{Si}} = 465.2 \text{ mm}$  [76].  
1054 The average value of  $r_\chi = \frac{1}{2} \frac{\Delta\chi}{\Delta\lambda}$ , which governs the size of the matter regeneration  
1055 effect, can be calculated for the three considered experimental scenarios and satisfy  
1056  $|r_\chi^{\text{LL}}| = 2.7 \times 10^{-3}$ ,  $|r_\chi^{\text{DD}}| = 2.2 \times 10^{-3}$ , and  $|r_\chi^{\text{Belle II}}| = 1.0 \times 10^{-3}$ .

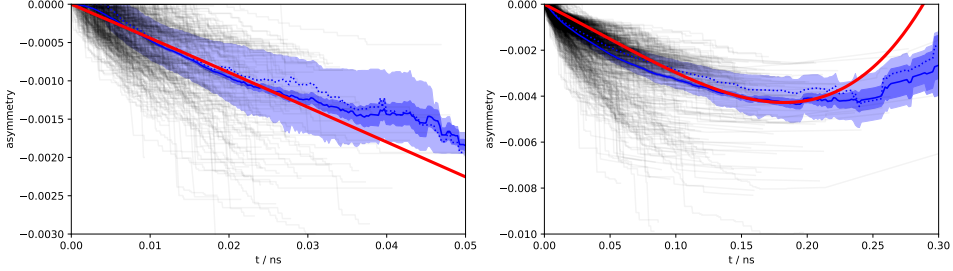


**Figure 3.5:** The asymmetry in Eq. (3.40) as a function of time for (left) LL and (right) DD  $K_S^0$  tracks in a simulated LHCb sample. The black lines show individual tracks. The light blue area is the central 50 % quantile, the dark blue area is the  $1\sigma$  uncertainty band on the mean. The red lines are calculated using the average  $\Delta\chi$  values that are also used in the calculation of biases in BPGGSZ measurements.

The neutral kaon tracks in LHCb generally pass through somewhere between zero (for a significant amount of the LL tracks) and a hundred (for some DD tracks) distinct detector segments. Therefore it is worth examining the degree to which using a single average  $\Delta\chi$  value, obtained following the procedure outlined above, provides a reasonable description of the average material interaction. This can be done using full LHCb simulation, where the kaon state for a simulated track can be evaluated at all times, by applying Eq. (3.15) iteratively for each detector segment the track traverses, using a  $\Delta\chi$  value appropriate for that segment. This is done in Fig. 3.5 for a simple observable: the yield asymmetry

$$A_{K^0} = \frac{|\psi_{K^0}(t)|^2 - |\psi_{\bar{K}^0}(t)|^2}{|\psi_{K^0}(t)|^2 + |\psi_{\bar{K}^0}(t)|^2}, \quad (3.40)$$

where  $\psi_{K^0}(t)$  ( $\psi_{\bar{K}^0}(t)$ ) is the amplitude for an initial  $K^0$  ( $\bar{K}^0$ ) to decay to two pions at time  $t$ . In this calculation, it is assumed that  $\epsilon = 0$  to isolate the material effect with no asymmetry contribution from the inherent  $CP$ -violation in the neutral kaon sector. While the track-by-track asymmetries are found to differ significantly depending on the exact detector segments a track intersects, the average asymmetry is seen to evolve smoothly as a function of decay time, and in reasonable agreement with the asymmetry value that is calculated using the average  $\Delta\chi$  values estimated above.

The LHCb detector is undergoing a significant upgrade prior to the start of the LHC Run 3. However, the material budget and geometry of the relevant sub-detectors will be similar to the sub-detectors used during Run 1 and 2 [94, 95]. Hence the results of this study will be valid for measurements during the upgrade phases of LHCb, even though the detector parameters presented in this section relate to the original LHCb detector.

<sup>1079</sup> **3.3.5 Calculation procedure**

<sup>1080</sup> The main idea in the bias study is to calculate the BPGBSZ bin yields including  
<sup>1081</sup> the full effect of neutral kaon  $CP$  violation and material, fit them using the default  
<sup>1082</sup> equations of Chapter 1, and obtain the bias  $\Delta\gamma = \gamma - \gamma^0$  due to the kaon effects not  
<sup>1083</sup> being considered in the parameter extraction. For the purpose of Ref. [2], a simple  
<sup>1084</sup> fit setup of a single  $B^\pm \rightarrow Dh^\pm$  mode is investigated, where the  $K_i$  parameters are  
<sup>1085</sup> determined in a control channel with the relevant experimental acceptance. This  
<sup>1086</sup> setup is modified in the study used to assign a systematic uncertainty on the LHCb  
<sup>1087</sup> measurement of Chapter 4, as described in Section 3.3.7 below.

<sup>1088</sup> In practice, the amplitude model for  $D^0 \rightarrow K_S^0 \pi^+ \pi^-$  decays in Ref. [51] is taken  
<sup>1089</sup> to represent the  $A_1(s_{+-})$  amplitude. Then  $A_2(s_{+-})$  is obtained as described in  
<sup>1090</sup> Section 3.2.2. In terms of  $A_1$  and  $A_2$ , the amplitudes  $A_{S(L)}^{(\bar{D})}(s_{+-})$  can be expressed  
<sup>1091</sup> and related via Eqs. (3.25) and (3.26), and the full signal decay amplitudes as a  
<sup>1092</sup> function of phase-space coordinates, time, and the material interaction parameter  
<sup>1093</sup>  $\Delta\chi$  can be calculated for a given set of input parameters  $(\gamma^0, r_B^0, \delta_B^0)$ . The squared  
<sup>1094</sup> decay amplitudes are then integrated over phase space and the kaon decay times  
<sup>1095</sup> to obtain the binned signal yield.

<sup>1096</sup> The signal yields depend on the momentum via the time-acceptance parameters  
<sup>1097</sup>  $\tau_1$  and  $\tau_2$ , and because the material interaction parameter  $\Delta\chi$  is momentum  
<sup>1098</sup> dependent. Therefore, the yields are averaged over the  $K_S^0$  momentum distributions  
<sup>1099</sup> of LHCb and Belle II.

<sup>1100</sup> The parameters  $x_\pm$  and  $y_\pm$  are determined by a maximum likelihood fit to the  
<sup>1101</sup> calculated yields, after which the fit result and covariance matrix are interpreted  
<sup>1102</sup> in terms of the physics parameters  $(\gamma, r_B, \delta_B)$  using another maximum likelihood  
<sup>1103</sup> fit [96]. In the fits, the  $K_i$  are obtained using the definition  $K_i = K_i^{\text{meas}} =$   
<sup>1104</sup>  $(N_i^D + N_{-i}^{\bar{D}})/(\sum_j N_j^D + N_{-j}^{\bar{D}})$ , in terms of the expected yields  $N_i^D$  ( $N_i^{\bar{D}}$ ) of a flavour-  
<sup>1105</sup> tagged  $D^0$  ( $\bar{D}^0$ ) decays in bin  $i$  of the  $D$  decay phase space, calculated as described  
<sup>1106</sup> above for  $r_B^0 = 0$ . This corresponds to experimentally measuring the  $K_i$  in a control  
<sup>1107</sup> channel, and takes the effect of neutral kaon  $CP$  violation and material interaction  
<sup>1108</sup> on  $K_i$  measurements into account, as well the experimental time acceptance. The  
<sup>1109</sup>  $(c_i, s_i)$  are calculated using  $A_1(s_{+-})$  and the experimental time acceptance is taken  
<sup>1110</sup> into account in this calculation as well.

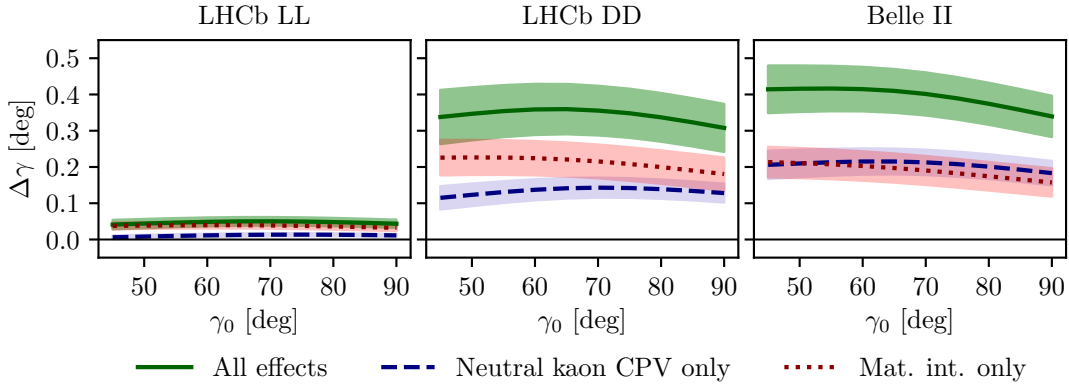


**Figure 3.6:** The bias  $\Delta\gamma$  as a function of input  $\gamma_0$  for (left) the LL LHCb category, (centre) the DD LHCb category, and (right) Belle II. The bias is calculated due to (blue, dashed line) neutral kaon  $CP$  violation alone, (red, dotted line) material interaction alone, and (green line) both effects. The shaded region shows the estimated  $1\sigma$  uncertainty band.

### 3.3.6 Results

The obtained bias  $\Delta\gamma$  is shown as a function of input  $\gamma^0$  for the various experimental conditions in Fig. 3.6. The calculations are made using  $(r_B^0, \delta_B^0) = (0.1, 130^\circ)$ , approximately equal to the physics parameters relevant for  $B^\pm \rightarrow DK^\pm$  decays [27, 39]. The bias does not vary significantly with  $\gamma^0$  in the plotted range, which includes the world average value of direct  $\gamma$  measurements as well as the values obtained in full unitarity-triangle fits [27, 38, 39], and for all cases, the bias is found to be below  $0.5^\circ$ , corresponding to relative biases of about half a percent. Thus the biases are of  $O(r\epsilon/r_B)$  as expected, given the arguments of Section 3.2.3. The contributions from the individual  $K_S^0$  CPV and material interaction effects are also shown. It is seen that the neutral kaon  $CP$  violation and material interaction effects leads to approximately equal biases in all three cases.

Given the decay-time acceptance and momentum distribution for each experimental category, the mean life time,  $\langle\tau\rangle$ , of the reconstructed kaons can be calculated. In terms of the  $K_S^0$  lifetime  $\tau_{K_S^0} = (0.895 \pm 0.004) \times 10^{-11}$  s [76],  $\langle\tau_{LL}\rangle \simeq 0.1\tau_{K_S^0}$  for the LHCb LL category,  $\langle\tau_{DD}\rangle \simeq 0.8\tau_{K_S^0}$  for the LHCb DD category, and at Belle II  $\langle\tau_{Belle\,II}\rangle \simeq \tau_{K_S^0}$ . The difference in average kaon lifetime is reflected in the observed biases, which are found to be larger in the samples with longer lived kaons. The very small effect in the LL category is to be expected because the  $CP$ -violation effect due to  $K_S^0$  not being  $CP$ -even is approximately cancelled by the  $CP$ -violation effect arising from  $K_S^0 - K_L^0$  interference for kaons with decay times much smaller than  $\tau_{K_S^0}$  [84].

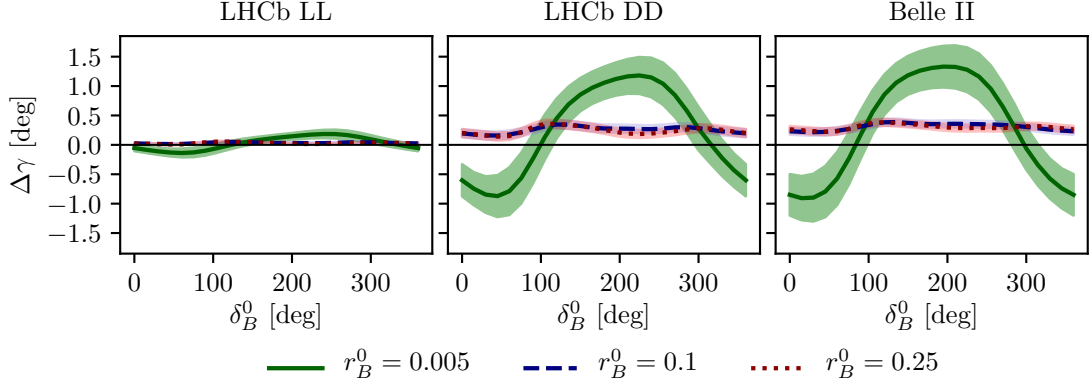


**Figure 3.7:** The bias  $\Delta\gamma$  as a function of input  $\delta_B$  for (left) the LL LHCb category, (centre) the DD LHCb category, and (right) Belle II. The bias is calculated for  $\gamma = 75^\circ$  and (green line)  $r_B = 0.005$ , (blue, dashed line)  $r_B = 0.1$ , and (red, dotted line)  $r_B = 0.25$ . The shaded region shows the estimated  $1\sigma$  uncertainty band.

1133 The uncertainty bands in Fig. 3.6 are calculated by repeating the study while  
 1134 varying some of the inputs. The model dependence of the predicted biases is  
 1135 probed by repeating the study using two other amplitude models as input for  
 1136  $A_1(s_{+-})$  and  $A_2$  [ ]: the model published in Ref. [61] and the model included in  
 1137 EVTGEN [97]. When defining  $A_2(s_{+-})$  in terms of  $A_1(s_{+-})$ , there is an uncertainty  
 1138 due to the unknown  $(r_k, \delta_k)$  parameters used to describe the  $\pi\pi$  resonance terms.  
 1139 This uncertainty is assessed by making the study with several different random  
 1140 realisations of the parameter set. The studies are repeated while varying the time  
 1141 acceptances and material densities with  $\pm 10\%$ . There is an additional uncertainty  
 1142 due to the use of simulation samples generated with **RapidSim** to describe the kaon  
 1143 momentum distribution, in lieu of full detector simulations.

1144 There is also an uncertainty from the use of  $(c_i, s_i)$  as calculated using  $A_1(s_{+-})$ .  
 1145 It is to be expected that the measured values  $(\hat{c}_i, \hat{s}_i)$  from the CLEO collaboration [ ]  
 1146 differ by those calculated using  $A_1^D(s_-, s_+)$  by terms of  $O(\epsilon)$  due to neutral kaon  
 1147  $CP$  violation, which is not taken into account in the measurement [69]. These  
 1148 corrections can be calculated via a procedure analogous to the one used to estimate  
 1149 the corrections on measurements of  $\gamma$  in this paper. However, as these corrections  
 1150 are much smaller than the experimental uncertainties in the measurement, they  
 1151 have not been studied further.

1152 For the purpose of this thesis, it is important to consider the bias in measurements  
 1153 that use  $B^\pm \rightarrow D\pi^\pm$  decays as well, and other  $B$  decay modes can also be used in  
 1154 BPFGSZ measurements, such as  $B^\pm \rightarrow D^*K^\pm$ ,  $B^\pm \rightarrow DK^{*\pm}$ , and  $B^0 \rightarrow DK^{*0}$ .  
 1155 For the purpose of the study presented here, the main difference between the decay

channels is that they have different values of  $r_B$  and  $\delta_B$ . Figure 3.7 shows  $\Delta\gamma$  as a function of input  $\delta_B^0$ , for  $\gamma^0 = 75^\circ$  and three different values of  $r_B^0$ . Aside from  $r_B^0 = 0.1$ , the results are shown for  $r_B^0 = 0.005$ , which corresponds to the expectation in  $B^\pm \rightarrow D\pi^\pm$  decays [47] and  $r_B^0 = 0.25$ , which corresponds to  $B^0 \rightarrow DK^{*0}$  decays [96, 98]. The most notable feature is that the biases are significantly larger in the  $B^\pm \rightarrow D\pi^\pm$  case. This is expected: the  $r_B^0$  dependent behaviour is governed by the relative importance of different  $O(r\epsilon)$  correction terms to the phase-space distribution. There are terms of both  $O(r_A\epsilon)$  and  $O(r_B\epsilon)^3$ , which lead to expected biases of size  $O(r_A\epsilon/r_B)$  and  $O(r_B\epsilon/r_B) = O(\epsilon)$ , respectively, cf. the discussion of Section 3.2.3. In the  $B^\pm \rightarrow D\pi^\pm$  case, the  $O(r_A\epsilon)$  correction terms dominate because  $r_A/r_B \simeq (0.05/0.005) = 10$ . This explains the relatively large bias, as  $|r_A\epsilon/r_B^{D\pi}| \simeq 4\%$ . The bias is seen to be up to  $\pm 1.5^\circ$ , but only about  $+0.2^\circ$  with the expected value of  $\delta_B^{D\pi} \simeq 300^\circ$  [47, 96]. These biases are *much smaller* than the precision on  $\gamma$  that is obtainable in a  $B^\pm \rightarrow D\pi^\pm$  analysis with current experimental yields, and do thus not pose a problem. In the  $r_B^0 = 0.1$  and  $r_B^0 = 0.25$  cases the  $O(r_B\epsilon)$  correction terms dominate, and the biases are of  $O(\epsilon)$ , independent of the  $r_B^0$  value. Therefore both cases have biases of similar size.

Further, it is clear that the biases depend on  $\delta_B^0$  and that the oscillation period of the  $\delta_B$  dependence is different between the  $r_B^0 = 0.005$  case and the  $r_B^0 \in \{0.1, 0.25\}$  cases. It is to be expected that  $\Delta\gamma$  oscillates as a function of  $\delta_B^0$ , because  $\delta_B^0$  enters the yield equations via  $\cos(\delta_B^0 \pm \gamma)$  and  $\sin(\delta_B^0 \pm \gamma)$  terms. As explained above, the  $O(r_A\epsilon)$  terms dominate the  $B^\pm \rightarrow D\pi^\pm$  bias, and these are independent of  $\delta_B^0$ . The  $O(r_B\epsilon)$  terms, however, are important for the bias corrections for larger  $r_B$  values, and the terms include factors of  $\cos(\delta_B^0 \pm \gamma)$  and  $\sin(\delta_B^0 \pm \gamma)$ . This explains the different bias dependence on  $\delta_B^0$ .

While the input value of  $\gamma^0 = 75^\circ$  was chosen for these studies, there is minimal variation in the results if another value of  $\gamma^0$  in the range  $[60^\circ, 85^\circ]$  is used.

### 3.3.7 Coupled $B^\pm \rightarrow DK^\pm$ and $B^\pm \rightarrow D\pi^\pm$ measurements

The studies presented above have been extended on two accounts in order to assign a systematic uncertainty to the LHCb measurement presented in Chapter 4. Firstly, full LHCb simulation has been used to obtain the momentum distributions, as well as to fit a better description of the time acceptance and the reconstruction efficiency profile over the  $D$ -decay phase space. Secondly, the fit setup is modified

---

<sup>3</sup>There are similar terms of  $O(r_A r_\chi)$  and  $O(r_B r_\chi)$ , but as  $\epsilon$  and  $r_\chi$  are of the same order of magnitude, these terms can be treated completely analogously to the  $O(r_A\epsilon)$  and  $O(r_B\epsilon)$  terms, and have been left out of the discussion for brevity.

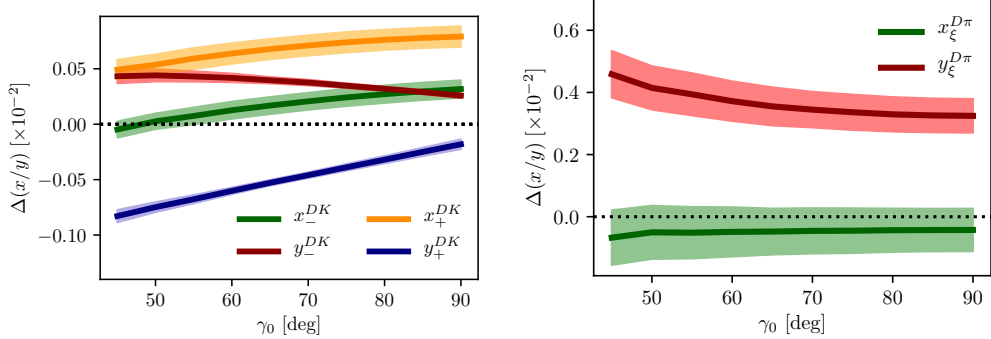


**Figure 3.8:** The bias on (left) the  $B^\pm \rightarrow DK^\pm$  and (right)  $B^\pm \rightarrow D\pi^\pm$   $CP$ -violation observables in the LHCb DD category, evaluated in bias studies with inputs based on full LHCb simulation, calculated as a function of input  $\gamma_0$ .

to correspond to the experimental approach described in Section 1.4 and Chapter 4: the signal yields are calculated for both the  $B^\pm \rightarrow DK^\pm$  and  $B^\pm \rightarrow D\pi^\pm$  channels, and fitted in a combined fit to obtain  $(x_\pm^{DK}, y_\pm^{DK}, x_\xi^{D\pi}, y_\xi^{D\pi})$ , where the  $F_i$  parameters are allowed to float in the fit. The biases obtained for each observable are shown in Fig. 3.8, evaluated using the time-acceptance, momentum distribution, and material budget relevant for the DD category (since the effect in the LL category is much smaller). As will be clear in Chapter 4, these biases are all significantly smaller than the corresponding statistical uncertainties. Thus, the effects of neutral kaon  $CP$  violation and material interactions contribute a manageable systematic uncertainty in current BPGGSZ measurements, even if the  $B^\pm \rightarrow D\pi^\pm$  channel is promoted to a signal channel.

As the statistical uncertainty becomes comparable with the bias effects described in this chapter, the systematic uncertainty should be assigned by a more accurate study, incorporating the traversed material on a track-by-track basis in full detector simulation. Such a detailed calculations can also be used to apply a bias correction if desired.

### 3.4 Concluding remarks

The analysis presented in this chapter has shown the expected impact of neutral kaon  $CP$  violation and material interaction on current BPGGSZ measurements to be small compared to the statistical uncertainties; first by simple order-of-magnitude estimates and then by a detailed calculation of the expected effect in LHCb and Belle II.

While the calculations were made for the case of  $D \rightarrow K_S^0 \pi^+ \pi^-$  decays, the BPGGSZ approach can of course also be applied in other  $D$ -decay final states,

such as  $D \rightarrow K_S^0 K^+ K^-$  and  $D \rightarrow K_S^0 \pi^+ \pi^- \pi^0$ . The biases on measurements of  $\gamma$  based the  $D$  decay phase-space distributions should be of similar size in these decay channels. The impact on  $\gamma$  measurements based on the phase-space-integrated yield asymmetry can be expected to be tens of degrees for the  $D \rightarrow K_S^0 K^+ K^-$  channel, where the yield asymmetry is expected to be around 2 %, for the reasons explained in Section 3.2.3. The  $D \rightarrow K_S^0 \pi^+ \pi^- \pi^0$  decay, however, is dominantly  $CP$ -odd [99], and the bias in measurements based on the total asymmetry is therefore expected to be  $O(\epsilon/r_B)$ , ie. a few degrees [74]. More precise calculations of the biases would require a repeat of the study included here, with relevant amplitude models and binning schemes in place.

The chapter focuses on the model-independent, binned approach that is the subject of the thesis. However, the underlying mechanism that determines the scale of the bias, namely that the phase-space *distribution* of signal decays is unaffected at  $\mathcal{O}(\epsilon)$  and  $\mathcal{O}(r_\chi)$ , is independent on the exact measurement approach. Therefore it is expected that amplitude-model-based measurements and measurements made with new unbinned methods such as those in Ref [68] will be similarly biased if kaon  $CP$  violation and regeneration are not accounted for.

# 4

1230

1231 A GGSZ measurement with  $B^\pm \rightarrow Dh^\pm$   
1232 decays

1233 First I will return to describing the overall strategy a bit, then one can proceed  
1234 with the data analysis section

1235 **4.1 Candidate selection**

1236 **4.2 Signal and background components**

1237 **4.3 Measurement of the CP-violation observables**

1238 **4.4 Systematic uncertainties**

1239 **4.5 Obtained constraints on  $\gamma$**

1240

## Bibliography

- 1241 [1] LHCb collaboration, R. Aaij *et al.*, *Measurement of the CKM angle  $\gamma$  using*  
 1242  $B^\pm \rightarrow [K_S^0 h^+ h^-]_D h^\pm$  *decays*, Submitted to JHEP (2020).
- 1243 [2] M. Bjørn and S. Malde, *CP violation and material interaction of neutral*  
 1244 *kaons in measurements of the CKM angle  $\gamma$  using  $B^\pm \rightarrow DK^\pm$  decays where*  
 1245  $D \rightarrow K_S^0 \pi^+ \pi^-$ , JHEP **19** (2020) 106, arXiv:1904.01129.
- 1246 [3] LHCb collaboration, R. Aaij *et al.*, *Measurement of the CKM angle  $\gamma$  using*  
 1247  $B^\pm \rightarrow DK^\pm$  *with  $D \rightarrow K_S^0 \pi^+ \pi^-$ ,  $K_S^0 K^+ K^-$  decays*, JHEP **08** (2018) 176,  
 1248 Erratum ibid. **10** (2018) 107, arXiv:1806.01202.
- 1249 [4] E. Noether, *Invariante Variationsprobleme*, Nachrichten von der Gesellschaft  
 1250 der Wissenschaften zu Göttingen, Mathematisch-Physikalische Klasse **1918**  
 1251 (1918) 235.
- 1252 [5] J. F. Donoghue, E. Golowich, and B. R. Holstein, *Dynamics of the Standard*  
 1253 *Model*, Cambridge University Press, Cambridge, 2014.
- 1254 [6] A. D. Sakarov, *Violation of CP Invariance, C Asymmetry, and Baryon*  
 1255 *Asymmetry of the Universe*, JETP Letters **5** (1966) 24.
- 1256 [7] G. Luders, *On the Equivalence of Invariance under Time Reversal and under*  
 1257 *Particle-Antiparticle Conjugation for Relativistic Field Theories*, Kong. Dan.  
 1258 Vid. Sel. Mat. Fys. Medd. **28N5** (1954) 1.
- 1259 [8] C. S. Wu *et al.*, *Experimental Test of Parity Conservation in Beta Decay*,  
 1260 Physical Review **105** (1957) 1413.
- 1261 [9] T. D. Lee and C. N. Yang, *Question of Parity Conservation in Weak*  
 1262 *Interactions*, Physical Review **104** (1956) 254.
- 1263 [10] J. H. Christenson, J. W. Cronin, V. L. Fitch, and R. Turlay, *Evidence for the*  
 1264  $2\pi$  *Decay of the  $K_2^0$  Meson*, Physical Review Letters **13** (1964) 138.

- 1265 [11] BABAR Collaboration *et al.*, *Observation of  $\mathit{CP}$  Violation in the*
- 1266  $\mathit{B}^0$  Meson System, Physical Review Letters **87** (2001) 091801.
- 1267 [12] Belle Collaboration *et al.*, *Observation of Large  $\mathit{CP}$  Violation in*
- 1268 *the Neutral  $\mathit{B}$  Meson System*, Physical Review Letters **87** (2001)
- 1269 091802.
- 1270 [13] K. Abe, *Study of  $B^{+-} \rightarrow D_{\text{CP}} K^{+-}$  and  $D^{\ast}_{\text{CP}} K^{+-}$  decays*, Physical
- 1271 Review D **73** (2006) 051106, arXiv:hep-ex/0601032.
- 1272 [14] B. Collaboration *et al.*, *Evidence for the Suppressed Decay  $B^- \rightarrow DK^-$ ,  $D \rightarrow$*
- 1273  *$K + pi^-$* , Physical Review Letters **106** (2011) 231803, arXiv:1103.5951.
- 1274 [15] T. B. Collaboration and P. d. A. Sanchez, *Measurement of  $CP$  observables*
- 1275 *in  $B^{+-} \rightarrow D_{\text{CP}} K^{+-}$  decays and constraints on the CKM angle gamma*,
- 1276 Physical Review D **82** (2010) 072004, arXiv:1007.0504.
- 1277 [16] The BABAR Collaboration *et al.*, *Search for*
- 1278  $b \rightarrow D_s^+ \pi^-$  transitions *in*  $B^0 \rightarrow D_s^+ \pi^-$  and
- 1279  $D_s^+ \rightarrow D^+ \pi^0$  decays, Physical Review D **82** (2010)
- 1280 072006.
- 1281 [17] C. Collaboration, *Measurements of branching fraction ratios and  $CP$  asymmetries in  $B^{+-} \rightarrow D_{\text{CP}} K^{+-}$  decays in hadron collisions*, Physical Review D **81** (2010) 031105, arXiv:0911.0425.
- 1282 [18] C. Collaboration, *Measurements of branching fraction ratios and  $CP$ -asymmetries in suppressed  $B^\pm \rightarrow D(\rightarrow K \pi)K^\pm$  and  $B^\pm \rightarrow D(\rightarrow K \pi)pi^\pm$  decays*, Physical Review D **84** (2011) 091504, arXiv:1108.5765.
- 1283 [19] LHCb collaboration, R. Aaij *et al.*, *Observation of  $CP$  violation in  $B^\pm \rightarrow DK^\pm$  decays*, Phys. Lett. **B712** (2012) 203, Erratum ibid. **B713** (2012) 351, arXiv:1203.3662.
- 1284 [20] LHCb collaboration, R. Aaij *et al.*, *First observation of  $CP$  violation in the decays of  $B_s^0$  mesons*, Phys. Rev. Lett. **110** (2013) 221601, arXiv:1304.6173.
- 1285 [21] LHCb collaboration, R. Aaij *et al.*, *Observation of  $CP$  violation in neutral D-meson decays*, LHCb-PAPER-2019-006, in preparation.

- 1295 [22] K. Abe *et al.*, *Constraint on the matter–antimatter symmetry-violating phase*  
1296 *in neutrino oscillations*, Nature **580** (2020) 339.
- 1297 [23] L. K. Gibbons *et al.*, *Measurement of the CP-violation parameter*  
1298  $\text{Re}(\text{varepsilon}/\text{varepsilon})$ , Physical Review Letters **70** (1993) 1203.
- 1300 [24] G. D. Barr *et al.*, *A new measurement of direct CP violation in the neutral*  
1301 *kaon system*, Physics Letters B **317** (1993) 233.
- 1302 [25] J. R. Batley *et al.*, *A precision measurement of direct CP violation in the decay*  
1303 *of neutral kaons into two pions*, Physics Letters B **544** (2002) 97.
- 1304 [26] KTeV Collaboration *et al.*, *Measurements of direct  $\mathcal{CP}$  violation,*  
1305  *$\mathcal{CPT}$  symmetry, and other parameters in the neutral kaon system*,  
1306 Physical Review D **67** (2003) 012005.
- 1307 [27] HFLAV, Y. S. Amhis *et al.*, *Averages of b-hadron, c-hadron, and  $\tau$ -lepton*  
1308 *properties as of 2018*, arXiv:1909.12524, updated results and plots available  
1309 at <https://hflav.web.cern.ch/>.
- 1310 [28] M. Kobayashi and T. Maskawa, *CP-Violation in the Renormalizable Theory of*  
1311 *Weak Interaction*, Progress of Theoretical Physics **49** (1973) 652.
- 1312 [29] N. Cabibbo, *Unitary Symmetry and Leptonic Decays*, Physical Review Letters  
1313 **10** (1963) 531.
- 1314 [30] L.-L. Chau and W.-Y. Keung, *Comments on the Parametrization of the*  
1315 *Kobayashi-Maskawa Matrix*, Physical Review Letters **53** (1984) 1802.
- 1316 [31] Particle Data Group, M. Tanabashi *et al.*, *Review of particle physics*, Phys.  
1317 Rev. **D98** (2018) 030001, and 2019 update.
- 1318 [32] L. Wolfenstein, *Parametrization of the Kobayashi-Maskawa Matrix*, Physical  
1319 Review Letters **51** (1983) 1945.
- 1320 [33] Y. H. Ahn, H.-Y. Cheng, and S. Oh, *Wolfenstein parametrization at higher*  
1321 *order: Seeming discrepancies and their resolution*, Physics Letters B **703** (2011)  
1322 571.

- [34] A. J. Buras, M. E. Lautenbacher, and G. Ostermaier, *Waiting for the top quark mass, mixing, and CP asymmetries in B decays*, Physical Review D **50** (1994) 3433.
- [35] J. Charles *et al.*, *CP violation and the CKM matrix: Assessing the impact of the asymmetric B factories*, The European Physical Journal C - Particles and Fields **41** (2005) 1.
- [36] J. Brod and J. Zupan, *The ultimate theoretical error on  $\gamma$  from  $B \rightarrow DK$  decays*, Journal of High Energy Physics **2014** (2014) 51.
- [37] M. Blanke and A. J. Buras, *Emerging  $\Delta M_d$ -anomaly from tree-level determinations of  $V_{cb}$  and the angle  $\gamma$* , The European Physical Journal C **79** (2019) 159.
- [38] CKMfitter group, J. Charles *et al.*, *Current status of the Standard Model CKM fit and constraints on  $\Delta F = 2$  new physics*, Phys. Rev. **D91** (2015) 073007, arXiv:1501.05013, updated results and plots available at <http://ckmfitter.in2p3.fr/>.
- [39] UTfit collaboration, M. Bona *et al.*, *The unitarity triangle fit in the standard model and hadronic parameters from lattice QCD: A reappraisal after the measurements of  $\Delta m_s$  and  $BR(B \rightarrow \tau\nu_\tau)$* , JHEP **10** (2006) 081, arXiv:hep-ph/0606167, updated results and plots available at <http://www.utfit.org/>.
- [40] E. Kou *et al.*, *The Belle II Physics Book*, Progress of Theoretical and Experimental Physics **2019** (2019) 123C01, arXiv:1808.10567.
- [41] LHCb collaboration *et al.*, *Physics case for an LHCb Upgrade II - Opportunities in flavour physics, and beyond, in the HL-LHC era*, arXiv:1808.08865 [hep-ex] (2019) arXiv:1808.08865.
- [42] Y. Grossman and M. Savastio, *Effects of  $K\bar{K}$ - $\{\overline{K}\bar{K}\}$  mixing on determining  $\gamma$  from  $B^\pm \rightarrow DK^\pm$* , Journal of High Energy Physics **2014** (2014) 8.
- [43] M. Gronau and D. Wyler, *On determining a weak phase from charged B decay asymmetries*, Physics Letters B **265** (1991) 172.

- 1355 [44] M. Gronau and D. London, *How to determine all the angles of the unitarity*  
 1356 *triangle from  $Bd0 \rightarrow DKs$  and  $Bs0 \rightarrow D\phi$* , Physics Letters B **253** (1991)  
 1357 483.
- 1358 [45] D. Atwood, I. Dunietz, and A. Soni, *Enhanced CP Violation with*  
 1359  *$\mathcal{B} \rightarrow D\bar{D}$  Modes and Extraction of the Cabibbo-Kobayashi-Maskawa Angle*  
 1360  *$\gamma$* , Physical Review Letters **78** (1997) 3257.
- 1362 [46] D. Atwood, I. Dunietz, and A. Soni, *Improved*  
 1363 *methods for observing CP violation in*  
 1364  *$\mathcal{B} \rightarrow D\bar{D}$  and measuring the CKM phase  $\gamma$* , Physical Review D  
 1365 **63** (2001) 036005.
- 1367 [47] M. Kenzie, M. Martinelli, and N. Tuning, *Estimating*  
 1368  *$r_B$  as an input to the determination of*  
 1369 *the CKM angle  $\gamma$* , Physical Review D **94** (2016)  
 1370 054021.
- 1371 [48] T. Evans, J. Libby, S. Malde, and G. Wilkinson, *Improved sensitivity to the*  
 1372 *CKM phase  $\gamma$  through binning phase space in  $B^- \rightarrow DK^-$ ,  $D \rightarrow K\pi - \pi - \pi +$*   
 1373 *decays*, Physics Letters B **802** (2020) 135188.
- 1374 [49] S. Harnew *et al.*, *Model-independent determination of the strong phase difference*  
 1375 *between  $D0$  and  $D^- \rightarrow \pi^+ \pi^- \pi^+ \pi^-$  amplitudes*, Journal of High Energy Physics **2018** (2018)  
 1376 144.
- 1378 [50] R. H. Dalitz, *CXII. On the analysis of  $\tau$ -meson data and the nature of the*  
 1379  *$\tau$ -meson*, The London, Edinburgh, and Dublin Philosophical Magazine and  
 1380 *Journal of Science* **44** (1953) 1068.
- 1381 [51] BaBar Collaboration *et al.*, *Measurement of*  
 1382  *$\cos 2\beta$  in  $B^0 \rightarrow D^+ \bar{D}^-$  decays by a combined time-dependent Dalitz plot analysis of BaBar and*  
 1383 *Belle data*, Physical Review D **98** (2018) 112012.
- 1386 [52] S. U. Chung *et al.*, *Partial wave analysis in K-matrix formalism*, Annalen der  
 1387 Physik **507** (1995) 404.

- 1388 [53] D. Aston *et al.*, *A study of  $K\pi+$  scattering in the reaction  $Kp \rightarrow K\pi+n$  at 11*  
 1389 *GeV/c*, Nuclear Physics B **296** (1988) 493.
- 1390 [54] A. Bondar, *Proceedings of BINP special analysis meeting on Dalitz analysis,*  
 1391 *24-26 Sep. 2002, unpublished.*
- 1392 [55] A. Giri, Y. Grossman, A. Soffer, and J. Zupan, *Determining  $\gamma$  using*  
 1393  *$B$  decays, Physical Review D **68** (2003) 054018.*
- 1394  *$B$  decays with multibody  $D$  decays, Physical Review D **68** (2003) 054018.*
- 1395 [56] BaBar collaboration, B. Aubert *et al.*, *Measurement of the Cabibbo-Kobayashi-Maskawa angle  $\gamma$  in  $B^\mp \rightarrow D^{(*)}K^\mp$  decays with a Dalitz analysis of  $D \rightarrow K_S^0\pi^-\pi^+$* , Phys. Rev. Lett. **95** (2005) 121802, [arXiv:hep-ex/0504039](https://arxiv.org/abs/hep-ex/0504039).
- 1396 [57] BaBar collaboration, B. Aubert *et al.*, *Improved measurement of the CKM angle  $\gamma$  in  $B^\mp \rightarrow D^{(*)}K^{(*)\mp}$  decays with a Dalitz plot analysis of  $D$  decays to  $K_S^0\pi^+\pi^-$  and  $K_S^0K^+K^-$* , Phys. Rev. **D78** (2008) 034023, [arXiv:0804.2089](https://arxiv.org/abs/0804.2089).
- 1397 [58] BaBar collaboration, P. del Amo Sanchez *et al.*, *Evidence for direct CP violation in the measurement of the Cabibbo-Kobayashi-Maskawa angle  $\gamma$  with  $B^\mp \rightarrow D^{(*)}K^{(*)\mp}$  decays*, Phys. Rev. Lett. **105** (2010) 121801, [arXiv:1005.1096](https://arxiv.org/abs/1005.1096).
- 1398 [59] Belle collaboration, A. Poluektov *et al.*, *Measurement of  $\phi_3$  with Dalitz plot analysis of  $B^\pm \rightarrow D^{(*)}K^\pm$  decay*, Phys. Rev. **D70** (2004) 072003, [arXiv:hep-ex/0406067](https://arxiv.org/abs/hep-ex/0406067).
- 1399 [60] Belle collaboration, A. Poluektov *et al.*, *Measurement of  $\phi_3$  with Dalitz plot analysis of  $B^+ \rightarrow D^{(*)}K^{(*)+}$  decay*, Phys. Rev. **D73** (2006) 112009, [arXiv:hep-ex/0604054](https://arxiv.org/abs/hep-ex/0604054).
- 1400 [61] Belle collaboration, A. Poluektov *et al.*, *Evidence for direct CP violation in the decay  $B^\pm \rightarrow D^{(*)}K^\pm$ ,  $D \rightarrow K_S^0\pi^+\pi^-$  and measurement of the CKM phase  $\phi_3$* , Phys. Rev. **D81** (2010) 112002, [arXiv:1003.3360](https://arxiv.org/abs/1003.3360).
- 1401 [62] LHCb collaboration, R. Aaij *et al.*, *Measurement of CP violation and constraints on the CKM angle  $\gamma$  in  $B^\pm \rightarrow DK^\pm$  with  $D \rightarrow K_S^0\pi^+\pi^-$  decays*, Nucl. Phys. **B888** (2014) 169, [arXiv:1407.6211](https://arxiv.org/abs/1407.6211).
- 1402 [63] LHCb collaboration, R. Aaij *et al.*, *Measurement of the CKM angle  $\gamma$  using  $B^0 \rightarrow DK^{*0}$  with  $D \rightarrow K_S^0\pi^+\pi^-$  decays*, JHEP **08** (2016) 137, [arXiv:1605.01082](https://arxiv.org/abs/1605.01082).

- [64] A. Bondar and A. Poluektov, *Feasibility study of model-independent approach to  $\Phi 3$  measurement using Dalitz plot analysis*, The European Physical Journal C - Particles and Fields **47** (2006) 347.
- [65] A. Bondar and A. Poluektov, *The use of quantum-correlated  $D0$  decays for  $\Phi 3$  measurement*, The European Physical Journal C **55** (2008) 51.
- [66] Belle collaboration, H. Aihara *et al.*, *First measurement of  $\phi_3$  with a model-independent Dalitz plot analysis of  $B^\pm \rightarrow DK^\pm$ ,  $D \rightarrow K_S^0\pi^+\pi^-$  decay*, Phys. Rev. **D85** (2012) 112014, [arXiv:1204.6561](https://arxiv.org/abs/1204.6561).
- [67] LHCb collaboration, R. Aaij *et al.*, *A model-independent Dalitz plot analysis of  $B^\pm \rightarrow DK^\pm$  with  $D \rightarrow K_S^0 h^+ h^-$  ( $h = \pi, K$ ) decays and constraints on the CKM angle  $\gamma$* , Phys. Lett. **B718** (2012) 43, [arXiv:1209.5869](https://arxiv.org/abs/1209.5869).
- [68] A. Poluektov, *Unbinned model-independent measurements with coherent admixtures of multibody neutral  $D$  meson decays*, The European Physical Journal C **78** (2018) 121.
- [69] CLEO Collaboration *et al.*, *Model-independent determination of the strong-phase difference between  $\hat{D}^0$  and  $\hat{\overline{D}}^0$  and its impact on the measurement of the CKM angle  $\gamma$* , Physical Review D **82** (2010) 112006.
- [70] M. Ablikim *et al.*, *Model-independent determination of the relative strong-phase difference between  $D\bar{D}$  and  $\bar{D}\bar{D}$  and its impact on the measurement of the CKM angle  $\gamma$* , arXiv:2003.00091 [hep-ex] (2020) [arXiv:2003.00091](https://arxiv.org/abs/2003.00091).
- [71] R. Aaij *et al.*, *Near-threshold  $DD^-$  spectroscopy and observation of a new charmonium state*, Journal of High Energy Physics **2019** (2019) 35.
- [72] C. Thomas and G. Wilkinson, *Model-independent  $D\bar{D}$ -mixing and CP violation studies with  $D\bar{D}$  to  $K_S\pi^+\pi^-$  and  $D\bar{D}$  to  $K_S\hat{K}$* , Journal of High Energy Physics **2012** (2012) 185.

- [73] LHCb collaboration, R. Aaij *et al.*, *Measurement of the CKM angle  $\gamma$  using  $B^\pm \rightarrow DK^\pm$  with  $D \rightarrow K_S^0\pi^+\pi^-$ ,  $K_S^0K^+K^-$  decays*, JHEP **10** (2014) 097, arXiv:1408.2748.
- [74] Y. Grossman and M. Savastio, *Effects of  $K - \bar{K}$  mixing on determining gamma from  $B \hat{\rightarrow} DK$* , Journal of High Energy Physics **2014** (2014) , arXiv:1311.3575.
- [75] J. Garra Ticó, *A strategy for a simultaneous measurement of CP violation parameters related to the CKM angle  $\gamma$  in multiple B meson decay channels*, arXiv:1804.05597.
- [76] Particle Data Group, P. A. Zyla *et al.*, *Review of particle physics*, Prog. Theor. Exp. Phys **2020** (2020) 083C01.
- [77] A. Pais and O. Piccioni, *Note on the Decay and Absorption of the  $\theta$* , Physical Review **100** (1955) 1487.
- [78] M. L. Good, *Relation between Scattering and Absorption in the Pais-Piccioni Phenomenon*, Physical Review **106** (1957) 591.
- [79] W. Fetscher *et al.*, *Regeneration of arbitrary coherent neutral kaon states: A new method for measuring the  $K\bar{K}$  forward scattering amplitude*, Zeitschrift für Physik C: Particles and Fields **72** (1996) 543.
- [80] E. Kou *et al.*, *The Belle II Physics Book*, Progress of Theoretical and Experimental Physics **2019** (2019) 123C01, arXiv:1808.10567.
- [81] LHCb collaboration *et al.*, *Physics case for an LHCb Upgrade II - Opportunities in flavour physics, and beyond, in the HL-LHC era*, arXiv:1808.08865 [hep-ex] (2019) arXiv:1808.08865.
- [82] I. I. Bigi and H. Yamamoto, *Interference between Cabibbo allowed and doubly forbidden transitions in  $D \rightarrow KS, L + i's$  decays*, Physics Letters B **349** (1995) 363.
- [83] CLEO Collaboration *et al.*, *Comparison of  $D \rightarrow K\pi$  and  $D \rightarrow L\pi$  Decay Rates*, Physical Review Letters **100** (2008) 091801.

- 1483 [84] Y. Grossman and Y. Nir, *CP violation in  $T^\pm \rightarrow i^\pm KSv$  and  $D^\pm \rightarrow i^\pm KS$ :  
1484 The importance of  $KS$ -  $KL$ interference*, Journal of High Energy Physics **2012**  
1485 (2012) 2.
- 1486 [85] G. A. Cowan, D. C. Craik, and M. D. Needham, *RapidSim: An application  
1487 for the fast simulation of heavy-quark hadron decays*, Computer Physics  
1488 Communications **214** (2017) 239.
- 1489 [86] LHCb collaboration, *LHCb reoptimized detector design and performance:  
1490 Technical Design Report*, Tech. Rep. CERN-LHCC-2003-030, LHCB-TDR-9,  
1491 CERN, Geneva, 2003.
- 1492 [87] J. Gassner, M. Needham, and O. Steinkamp, *Layout and Expected Performance  
1493 of the LHCb TT Station*, Tech. Rep. LHCb-2003-140, CERN, Geneva, 2004.
- 1494 [88] Belle Collaboration, A. B. Kaliyar *et al.*, *Measurements of branching fraction  
1495 and direct cp asymmetry in  $B^\pm \rightarrow K_S^0 K_S^0 K^\pm$  and a search for  $B^\pm \rightarrow K_S^0 K_S^0 \pi^\pm$* ,  
1496 Phys. Rev. D **99** (2019) 031102.
- 1497 [89] N. Hiroshi, *Search for new physics by a time-dependent CP violation analysis  
1498 of the decay  $B \rightarrow K_S^0$  eta gamma using the Belle detector*, PhD thesis, Tohoku  
1499 University, Senday, 2015.
- 1500 [90] A. Gsponer *et al.*, *Precise Coherent  $K_S^0$  Regeneration Amplitudes for C, Al,  
1501 Cu, Sn, and Pb Nuclei from 20 to 140 GeV/c and Their Interpretation*, Phys.  
1502 Rev. Lett. **22** (1979) 13.
- 1503 [91] R. A. Briere and B. Weinstein, *Determining the Phase of a Strong Scattering  
1504 Amplitude from Its Momentum Dependence to Better Than 1°: The Example  
1505 of Kaon Regeneration*, Phys. Rev. Lett. **75** (1995) 402.
- 1506 [92] B. R. Ko, E. Won, B. Golob, and P. Pakhlov, *Effect of nuclear interactions of  
1507 neutral kaons on cp asymmetry measurements*, Phys. Rev. D **84** (2011) 111501.
- 1508 [93] LHCb collaboration, *LHCb RICH1 Engineering Design Review Report*, Tech.  
1509 Rep. LHCb-2004-121, CERN, Geneva, 2004.
- 1510 [94] LHCb Collaboration, *LHCb VELO Upgrade Technical Design Report*, Tech.  
1511 Rep. CERN-LHCC-2013-021. LHCB-TDR-013, 2013.
- 1512 [95] LHCb Collaboration, *LHCb PID Upgrade Technical Design Report*, Tech. Rep.  
1513 CERN-LHCC-2013-022. LHCB-TDR-014, 2013.

- 1514 [96] LHCb collaboration, R. Aaij *et al.*, *Measurement of the CKM angle  $\gamma$  from a*
- 1515 combination of LHCb results, JHEP **12** (2016) 087, [arXiv:1611.03076](https://arxiv.org/abs/1611.03076).
- 1516 [97] D. J. Lange, *The EvtGen particle decay simulation package*, Nucl. Instrum.
- 1517 Meth. **A462** (2001) 152.
- 1518 [98] LHCb collaboration, M. W. Kenzie and M. P. Whitehead, *Update of the LHCb*
- 1519 *combination of the CKM angle  $\gamma$* , LHCb-CONF-2018-002, 2018.
- 1520 [99] P. K. Resmi, J. Libby, S. Malde, and G. Wilkinson, *Quantum-correlated mea-*
- 1521 *surements of  $D \rightarrow K_S^0 \pi^+ \pi^- \pi^0$  decays and consequences for the determination*
- 1522 *of the CKM angle  $\gamma$* , JHEP **01** (2018) 082, [arXiv:1710.10086](https://arxiv.org/abs/1710.10086).